Molecular Pharmacology Fast Forward. Published on September 26, 2018 as DOI: 10.1124/mol.118.113530
This article has not been copyedited and formatted. The final version may differ from this version.

1. Title page

Modeling and mutational analysis of the binding mode for the multimodal antidepressant drug vortioxetine to the human 5-HT_{3A} receptor

Lucy Kate Ladefoged[1], Lachlan Munro[2], Anders Juel Pedersen[2], Sarah C.R. Lummis[3], Benny Bang-Andersen[4], Thomas Balle[5], Birgit Schiøtt[1], Anders S. Kristensen[2]

Interdisciplinary Nanoscience Center (iNANO), Department of Chemistry, Aarhus University, Langelandsgade 140, DK-8000 Aarhus, Denmark
(LKL, BS)

Department of Drug Design and Pharmacology, University of Copenhagen, Universitetsparken 2, DK-2100 Copenhagen, Denmark
(LM, AJP, ASK)

Department of Biochemistry, University of Cambridge, Cambridge CB2 1QW, UK,
(SCRL)

Lundbeck Research, H. Lundbeck A/S, Ottiliavej 9, DK-2500 Valby, Denmark
(BBA)

Molecular Pharmacology Fast Forward. Published on September 26, 2018 as DOI: 10.1124/mol.118.113530
This article has not been copyedited and formatted. The final version may differ from this version.

Sydney School of Pharmacy, Faculty of Medicine and Health, The University of Sydney, Sydney, NSW 2006, Australia

(TB)

Molecular Pharmacology Fast Forward. Published on September 26, 2018 as DOI: 10.1124/mol.118.113530
This article has not been copyedited and formatted. The final version may differ from this version.

2. Running title page

Running title:

Binding of vortioxetine at the human 5-HT_{3A} receptor

Corresponding author information:

Birgit Schiøtt, Interdisciplinary Nanoscience Center (iNANO), Department of Chemistry, Aarhus University, Langelandsgade 140, DK-8000 Aarhus, Denmark, E-mail: birgit@chem.au.dk. Telephone: +45 87155975.

Anders S. Kristensen, Department of Drug Design and Pharmacology, University of Copenhagen, Universitetsparken 2, DK-2100 Copenhagen, Denmark. E-mail: ask@sund.ku.dk. Telephone: +45 35306505.

Text pages: 24

Tables: 3

Figures: 8

References: 59

Abstract: 175 words

Introduction: 747 words

Discussion: 1331 words

Abbreviations:

5-HT: 5-hydroxytryptamine, serotonin; 5-HTBP: 5-HT binding protein; AA: all-atom; AChBP: acetylcholine binding protein; CG: coarse grained; CI: confidence interval; CNS: central nervous system; cryoEM: cryo electron microscopy; DMEM: Dulbecco's modified Eagle's medium; ECD: extracellular domain; FBS: foetal bovine serum; $GABA_A$: γ-aminobutyric acid A; GlyR: glycine

Molecular Pharmacology Fast Forward. Published on September 26, 2018 as DOI: 10.1124/mol.118.113530
This article has not been copyedited and formatted. The final version may differ from this version.

receptor; h5-HT_{3A}: human 5-HT_{3A}; HEK-293: human embryonic kidney 293; hSERT: human SERT; ICD: intracellular domain; IFD: induced fit docking; m5-HT_{3A}: mouse 5-HT_{3A}; MM-PBSA: molecular mechanics – Poisson-Boltzmann and surface area; nAChR: nicotinic acetylcholine receptor; OR: oocyte recording; pLGIC: pentameric ligand-gated ion channel; RMSD: root-mean-square-deviation; SD: standard deviation; SERT: serotonin transporter; TMD: transmembrane domain; vdW: van der Waals; WT: wild type.

Molecular Pharmacology Fast Forward. Published on September 26, 2018 as DOI: 10.1124/mol.118.113530
This article has not been copyedited and formatted. The final version may differ from this version.

3. Abstract

5-HT_3 receptors are ligand-gated ion channels that mediate neurotransmission by serotonin in the central nervous system. Pharmacological inhibition of 5-HT_3 receptor activity has therapeutic potential in several psychiatric diseases, including depression and anxiety. The recently approved multimodal antidepressant vortioxetine has potent inhibitory activity at 5-HT_3 receptors. Vortioxetine has an inhibitory mechanism that differs from classical 5-HT_3 receptor competitive antagonists despite being believed to bind in the same binding site. Specifically, vortioxetine shows partial agonist activity followed by a persistent and insurmountable inhibition. We have investigated the binding mode of vortioxetine at the human 5-HT_{3A} receptor through computational and *in vitro* experiments to provide insight into the molecular mechanisms behind the unique pharmacological profile of the drug. We find that vortioxetine bind in a manner different from currently known 5-HT_{3A} orthosteric ligands. Specifically, while the binding pattern of vortioxetine mimics some aspects of both the setron class of competitive antagonists and 5-HT with regards to interactions with residues of the aromatic box motif in the orthosteric binding site, vortioxetine also form interactions with residues not previously described to be important for the binding of either setrons or 5-HT such as Thr176 and Val202 on loop B and F, respectively. Our results expand the framework for understanding how orthosteric ligands drive 5-HT_3 receptor function, which is of importance for the potential future development of novel classes of 5-HT_3 receptor antagonists.

Molecular Pharmacology Fast Forward. Published on September 26, 2018 as DOI: 10.1124/mol.118.113530
This article has not been copyedited and formatted. The final version may differ from this version.

4. Introduction

Serotonin (5-hydroxytryptamine, 5-HT) is a neurotransmitter that *via* ionotropic 5-HT_3 receptors, and a range of metabotropic receptors, regulates neural activities underlying a wide spectrum of basal as well as higher brain functions; including appetite, aggression, sleep, mood, and cognition (Berger et al., 2009). 5-HT_3 receptors belong to the pentameric ligand-gated ion channel (pLGICs) superfamily together with structurally and functionally related nicotinic acetylcholine- (nAChR), γ-aminobutyric acid A- ($GABA_A$) and glycine receptors (GlyR) (Barnes et al., 2009; Lummis, 2012; Nemecz et al., 2016; Nys et al., 2013). 5-HT_3 receptor inhibitors are in current use as anti-emetics and for the treatment of irritable bowel syndrome and are considered a potential therapy for anxiety-related behavior and cognitive decline in major depressive disorder and schizophrenia (Robertson et al., 1992; Thompson et al., 2006b).

Vortioxetine (Lu AA21004, Fig. 1C) is a multimodal antidepressant that acts as an inhibitor at the serotonin transporter (SERT), an agonist at 5-HT_{1A} receptors, a partial agonist at 5-HT_{1B} receptors, and an antagonist at 5-HT_{1D}, 5-HT_3 and 5-HT_7 receptors (Bang-Andersen et al., 2011; Sanchez et al., 2015). In addition to antidepressive effects, vortioxetine has been shown to improve aspects of cognitive function such as attention, processing speed, executive function, and memory (Mahableshwarkar et al., 2015; McIntyre et al., 2017; McIntyre et al., 2014), that may be linked to activity at 5-HT_3 receptors (Mork et al., 2013; Riga et al., 2016).

The molecular understanding of vortioxetine inhibition of 5-HT_3 receptors is currently limited. Vortioxetine is suggested to bind at the orthosteric binding site in 5-HT_{3A} receptors but differs in mechanism from other 5-HT_3 antagonists by having an initial partial

Molecular Pharmacology Fast Forward. Published on September 26, 2018 as DOI: 10.1124/mol.118.113530
This article has not been copyedited and formatted. The final version may differ from this version.

agonistic response followed by an apparently insurmountable inhibition of receptor function (Bang-Andersen et al., 2011; Dale et al., 2018). Thus, vortioxetine acts as a functional antagonist under steady-state conditions, though likely through a different mechanism to that of classical competitive 5-HT_3 antagonists (collectively known as setrons). The orthosteric binding site of 5-HT_3 receptors is formed at the interface between subunits in the extracellular domain (ECD) (Hassaine et al., 2014; Nemecz et al., 2016; Nys et al., 2013). As pentamers, five potential agonist binding sites exist in the 5-HT_3 receptor. Occupancy of one or two sites appear sufficient to drive conformational ECD rearrangements that trigger channel opening and subsequent entry to a desensitized conformation (Andersen et al., 2013; Corradi et al., 2009; Hibbs and Gouaux, 2011b; Rayes et al., 2009). Cryo electron microscopy (cryoEM) and X-ray crystal structures are available for eukaryotic pLGICs (Althoff et al., 2014; Du et al., 2015; Hibbs and Gouaux, 2011a; Huang et al., 2015; Huang et al., 2017; Miller and Aricescu, 2014; Morales-Perez et al., 2016; Unwin, 2005; Unwin and Fujiyoshi, 2012; Zuber and Unwin, 2013); including two structures of the mouse 5-HT_{3A} receptor (m5-HT_{3A}) (Hassaine et al., 2014; Basak et al., 2018). Furthermore, acetylcholine binding protein (AChBP) (Smit et al., 2001), a soluble eukaryotic protein that forms pentamers with an overall tertiary fold similar to the ECD of pLGICs (Brejc et al., 2001), has been engineered to acquire a 5-HT_3 receptor-like ligand profile (Kesters et al., 2013). This construct, denoted 5-HTBP (5-HT binding protein), allows for crystallographic analysis of 5-HT_3 receptor ligand binding (Kesters et al., 2013; Price et al., 2016; Price et al., 2015). Combined with computational, mutational, and biochemical analysis, structures provide insight into the molecular architecture of the 5-HT_3 receptor orthosteric binding site (Hassaine et al., 2014; Kesters et al., 2013), ligand

binding modes (Barbosa et al., 2010; Joshi et al., 2006; Kesters et al., 2013; Lochner and Thompson, 2016; Price et al., 2015; Price et al., 2016), and the potential conformational changes associated with ligand binding (Miller and Smart, 2010; Sander et al., 2010). From this and other work, a framework is emerging for understanding the molecular basis that underlies 5-HT_3 agonism and antagonism (Alix et al., 2016; Nys et al., 2013).

In the present study, we have studied the molecular basis of vortioxetine inhibition of human 5-HT_{3A} (h5-HT_{3A}) receptors by constructing a structural model of h5-HT_{3A}. This model is able to accurately predict the established binding mode of granisetron (Kesters et al., 2013; Ruepp et al., 2017), and was used for docking vortioxetine at the orthosteric binding site. We used pharmacological characterization of mutant receptors to identify and validate a model for vortioxetine in its bioactive conformation bound to the receptor. We find the location and conformation of vortioxetine in the binding site to be different from other known ligands, and this enables interactions with residues from both loop E and F simultaneously. Comparison with models for setron and agonist binding reveals distinct features for vortioxetine that might explain its unique inhibitory mechanism.

Molecular Pharmacology Fast Forward. Published on September 26, 2018 as DOI: 10.1124/mol.118.113530
This article has not been copyedited and formatted. The final version may differ from this version.

5. Materials and Methods

Materials – Chemicals were from Sigma (St. Louis, MO) except otherwise stated. Dulbecco's modified Eagle's medium (DMEM), fetal bovine serum (FBS), trypsin, and penicillin-streptomycin were from Invitrogen (Carlsbad, CA). DNA restriction enzymes were from New England Biolabs (Ipswich, MA). Cell culture dishes were from Sarstedt AG & Co (Nümbrecht, Germany), and 96-well plates were from VWR (Copenhagen, Denmark). Unlabeled and tritium labeled vortioxetine was provided by H. Lundbeck A/S (Valby, Denmark). [^{3}H]-GR65630 was from Perkin Elmer (Waltham, MA). DNA sequencing was performed using GATC Biotech (Constance, Germany). The FLIPR Blue membrane potential assay kit was from Molecular Devices (Sunnyvale, CA).

Molecular biology – cDNA encoding the h5-HT$_{3A}$ receptor was kindly provided by Dr. Beate Niesler, University of Heidelberg. The coding sequence for h5-HT$_{3A}$ was excised from the host vector pcDNA3.1 with *EcoR*I restriction enzyme and inserted into the combined mammalian and *Xenopus laevis* oocyte expression vector pXOON (Jespersen et al., 2002) in an *EcoR*I site in the multiple cloning site region using T4 DNA ligase (Roche, Germany). The resulting pXOON-h5-HT$_{3A}$ plasmid construct was confirmed by sequencing. Point mutations were generated by site-directed mutagenesis using the QuickChange mutagenesis kit (Stratagene, La Jolla, CA). All mutant constructs were verified by DNA sequencing (Eurofins Genomics, Ebersberg, Germany).

Xenopus laevis oocyte expression – Defoliated stage V to VI oocytes from *Xenopus laevis* were prepared as described previously (Poulsen et al., 2013) and injected with 15 ng mRNA. The care and use of *Xenopus laevis* was in strict adherence to a protocol (license 2014−15−0201−00031) approved by the Danish Veterinary and Food Administration that

Molecular Pharmacology Fast Forward. Published on September 26, 2018 as DOI: 10.1124/mol.118.113530
This article has not been copyedited and formatted. The final version may differ from this version.

is in accordance with the Guide for the Care and Use of Laboratory Animals adopted by the U.S. National Institutes of Health. Oocytes were incubated at 18 °C for 24 to 48 hours following injection. Recordings were made using a Warner OC725B two-electrode voltage clamp (Warner Instruments, Hamden, CT) configured as recommended by the manufacturer. For concentration-response experiments, oocytes were perfused with oocyte recording (OR) buffer (in mM: 115 NaCl, 2 KCl, 5 HEPES and 1.8 $BaCl_2$, pH 7.6) and ligands added by whole bath application using a PC-16 valve-based perfusion controller (Bioscience Tools, Highland, CA). For fast solution switching experiments used to determine receptor desensitization rates, solutions containing saturating concentrations of agonist were applied to the oocyte using a rapid perfusion scheme using a vertical flow chamber with a volume of 400 µL and a solution flow rate of 10 mL/min (Joshi et al., 2004). This approach allowed rapid switching between control and agonist-containing solutions that is essential to ensure resolution of desensitizing receptor currents. Solution exchange times was determined after each oocyte recording by stepping a dilute external solution across open electrode tips to measure a liquid junction current. The 10–90% rise times for solution exchange were consistent ~1 s or less. All experiments were performed at room temperature (23 °C). Data acquisitions were accomplished using a Digidata 1320A analog-digital converter (Molecular Devices, San Jose, CA) interfaced with a PC running WinWCP software (available from Strathclyde Electrophysiology Software, University of Strathclyde, Glasgow, UK).

Mammalian cell culturing and expression – Human embryonic kidney 293 (HEK-293) cells (American Type Culture Collection, Manassas, VA) were cultured in DMEM supplemented with 10% v/v fetal bovine serum, 100 units/ml penicillin, and 100 µg/ml

Molecular Pharmacology Fast Forward. Published on September 26, 2018 as DOI: 10.1124/mol.118.113530
This article has not been copyedited and formatted. The final version may differ from this version.

streptomycin) at 37 °C in a humidified 5% CO_2 environment. For expression of wild-type (WT) and mutant h5-HT_{3A} receptor, HEK-293 cells in suspension were transfected using TransIT DNA transfection reagent (Mirus, Madison, VA) according to the manufacturer instructions, plated into black 96-well clear bottom plates at a density of 30.000 cells/well and incubated for 48 hours before use.

Membrane potential assay – Concentration response experiments were performed using a FlexStation 1 microplate reader (Molecular Devices) essentially as described by Price and Lummis (Price and Lummis, 2005). Briefly, FLIPR blue membrane potential dye was diluted in assay buffer (denoted Flex50 and containing in mM: 57.5 NaCl, 57.5 NMDG+, 1 KCl, 1 $MgCl_2$, 1 $CaCl_2$, 10 HEPES and 10 glucose; adjusted to pH 7.4 with HCl) according to the manufacturer's instructions. Cells were incubated with 100 µL of the FLIPR blue loading solution per well at 37 ˚C for 30 minutes. Fluorescence in each well was measured in a FlexStation 1 (Molecular Devices) scanning plate-reading fluorometer with integrated automated pipettor at 2 s intervals for 200 s. At 18 seconds, 25 µL of 5-HT solution (in Flex50 buffer, final concentration 0.01 – 300 µM) was added to each well. For inhibitor concentration-response experiments, the inhibitor was included in the dye loading buffer during pre-incubation. Experiments on the N123L mutant were performed as described above, however using a modified assay buffer with increased NaCl concentration (denoted Flex100 and containing in mM: 115 NaCl, 1 KCl, 1 $MgCl_2$, 1 $CaCl_2$, 10 HEPES, and 10 Glucose; pH 7.4) in place of Flex50 buffer in order to increase signal amplitude due to lower responses with this mutant receptor. Experiments on WT h5-HT_{3A} receptors were performed in parallel using the Flex100 buffer and the IC_{50} values

Molecular Pharmacology Fast Forward. Published on September 26, 2018 as DOI: 10.1124/mol.118.113530
This article has not been copyedited and formatted. The final version may differ from this version.

identical to those seen in the Flex50 buffer were obtained. See *Supplementary Methods* for additional details.

Radioligand binding assay – Membranes from HEK-293 cells expressing h5-HT_{3A} receptors were prepared as described previously (Thompson et al., 2011). Briefly, a 10 cm dish of transfected HEK-293 cells were harvested by scraping into 1 mL ice-cold HEPES buffer (10 mM, pH 7.4) and frozen. Cells were then thawed, centrifuged at 20.000 g for 1 minute and the pellet was then resuspended in HEPES buffer. This procedure was repeated twice with a final resuspension in 2 mL HEPES buffer. For competition binding experiments, 50 µL suspensions of cell membranes were incubated in 500 µL HEPES buffer containing 0.3 nM [^{3}H]-GR65630 (equal to the K_d value for this radioligand) and varying concentrations of vortioxetine. Non-specific binding was determined by incubation with 10 µM quipazine. For saturation binding experiments, 50 µL of cell membranes were incubated in 500 µL HEPES buffer containing increasing concentrations of [^{3}H]-vortioxetine at 4 °C for 1 hr. For concentrations above 5 nM vortioxetine, [^{3}H]-vortioxetine was spiked with 2.5 nM unlabeled vortioxetine. Reactions were terminated by vacuum filtration using a Brandel (Gaithersburg, MD) cell harvester onto GF/B filters presoaked in 0.3% w/v polyethyleneimine. Radioactivity was determined by scintillation counting using a Beckman BCLS6500 instrument (Fullerton, CA).

Pharmacological data analysis – All data analyses involving iterative curve fitting were performed using GraphPad Prism software (GraphPad Inc., San Diego, CA, USA). In general for concentration-response data for EC_{50} or IC_{50} determinations, responses were defined as the change in fluorescence or current upon agonist stimulation and calculated as peak response (R_{peak}) minus baseline fluorescence or current (R_{base}) defined as fluorescence

Molecular Pharmacology Fast Forward. Published on September 26, 2018 as DOI: 10.1124/mol.118.113530
This article has not been copyedited and formatted. The final version may differ from this version.

or current immediately before agonist stimulation. For pooling of data from different experiments, we normalized responses according to the equation:

$$Normalized\ response = \frac{(Rpeak - Rbase)}{Rmax}$$

where *Rmax* is the fluorescence response recorded for application of a saturating concentration of 5-HT. For determination of IC_{50} and EC_{50} values, data were pooled among individual experiments and the composite concentration-inhibition data analyzed by iterative curve fitting using the equation:

$$Response = \frac{1}{(1 + 10^{(LogY - X)\times nH})}$$

where *Response* is the agonist-evoked response measured at a given inhibitor concentration normalized to the response in either absence of inhibitor (for IC_{50}) or the maximum response (for EC_{50}), Y is the concentration of inhibitor (for IC_{50}) or agonist (for EC_{50}) that produces a half-maximal inhibition or response, X is the logarithm of the concentration of the inhibitor or agonist concentration, and n_H is the Hill slope. For determination of the equilibrium dissociation constant (K_d) for vortioxetine from saturation radioligand binding experiments, specific binding data were analyzed by curve fitting according to the equation:

$$B = \frac{(Bmax \times [L])}{Kd + [L]}$$

where B is bound radioligand, $Bmax$ is maximum binding at equilibrium, K_d is the equilibrium dissociation constant, and $[L]$ is the free concentration of radioligand. For calculation of the inhibition constant (K_i) for vortioxetine from competition radioligand binding experiments, the Cheng-Prusoff equation (Cheng and Prusoff, 1973) was used

Molecular Pharmacology Fast Forward. Published on September 26, 2018 as DOI: 10.1124/mol.118.113530
This article has not been copyedited and formatted. The final version may differ from this version.

based on the assumption that vortioxetine and the radioligand bind competitively under steady-state conditions. Unless otherwise indicated, IC_{50} and EC_{50} values are shown with 95% confidence interval (CI), and statistical differences were analyzed using ANOVA followed by a Dunnett's Multiple Comparison Test using GraphPad Prism software.

Protein modeling – The h5-HT_{3A} receptor was modeled in an inactive conformation based on several templates as no single template of a cation-selective receptor in an unambiguously inactive conformation existed at the time of modeling. Therefore, the receptor was partly modelled based on the highly homologues m5-HT_{3A} (Hassaine et al., 2014). In this structure, the pore-lining helix, M2, is in an unclear conformational state as the conformation of the backbone is similar to other open channel receptor structures, while the conformations of the pore-lining side chains effectively close the pore (Hassaine et al., 2014). This was overcome by modelling in combination with a human $GABA_A$ receptor in an inactive conformation (Miller and Aricescu, 2014), and an antagonist-bound 5-HTBP (Kesters et al., 2013) using MODELLER 9.14 (Sali and Blundell, 1993)(Supplementary Methods)(Supplementary Figure S1).

Ligand preparation – The structure of granisetron was extracted from the crystal structure of 5-HTBP (PDB-ID: 2YME) while the structure of vortioxetine was prepared as described in Andersen *et al.* (Andersen et al., 2015). Following assignment of bond orders and atom types in Maestro 10.1 (Schrödinger Suite 2015), the granisetron structure was minimized and then subjected to a conformational search using the mixed torsional/low-mode sampling method, the OPLS 2.1 force field, and an implicit water model in MacroModel 10.7. A 5000 step minimization using a conjugate gradient method followed

Molecular Pharmacology Fast Forward. Published on September 26, 2018 as DOI: 10.1124/mol.118.113530
This article has not been copyedited and formatted. The final version may differ from this version.

each iteration step in the conformational search. Both ligands were modelled as having one charged amine based on available pK_a data.

Induced fit docking – Ligands were docked in their lowest energy conformation into each of the five substrate binding sites of h5-HT_{3A} using an induced fit docking (IFD) protocol. The protocol employed the Glide 6.4 and Prime 3.7 modules in the Schrödinger software suite (Schrödinger Suite 2015) that allows for full flexibility of both the ligand and binding site side chains (Friesner et al., 2004; Sherman et al., 2006). The binding site center was defined as the centroid of Trp178 and Ser226 in the principal subunit and Asp64 in the complementary subunit of each site. In the initial docking, Arg87 was mutated to alanine to allow room for the ligand, and a maximum of 200 poses were carried forward to the next step. A maximum of 100 ligand docking poses were reported in extra precision in the last docking step with energies less than 30 kcal/mol higher than the initial docking conformation. The resulting docking poses from each site were then combined and collectively clustered based on their in-place conformation using the Conformer Cluster script available in Maestro 10.1.

Molecular dynamics simulations – Simulation systems were set up and equilibrated using a coarse-grained (CG) approach before being converted into their all-atom (AA) equivalent for production run simulations. The receptor was placed in a solvated POPC bilayer and ionized to a 0.2 M NaCl concentration. CG simulations were performed using the MARTINI force field (Bulacu et al., 2013; de Jong et al., 2013) and AA simulations using the CHARMM36 force field (Best et al., 2012; Klauda et al., 2010). The *apo* receptor was simulated in the NPT ensemble in atomistic resolution for 10 ns with positional restraints on C_α atoms before docking calculations. Following the docking, a representative

Molecular Pharmacology Fast Forward. Published on September 26, 2018 as DOI: 10.1124/mol.118.113530
This article has not been copyedited and formatted. The final version may differ from this version.

pose from each cluster was simulated for 53.5 ns (1.5 ns of restrained equilibration, 2 ns of unrestrained pre-production equilibration, and 50 ns production run, respectively) (*Supplementary Methods*). The analyses were performed directly after the release of the restraints to assess the stability of the binding cluster as it was found in the IFD calculations. The root-mean-square-displacement (RMSD) of vortioxetine heavy atoms relative to their position in the first frame was monitored in each simulation as well as whether or not vortioxetine maintained its stabilizing interactions with the protein. See *Supplementary Methods* for simulation details and the parameterization of vortioxetine.

MM-PBSA calculations – The free energy of binding was estimated using the MM-PBSA method (Molecular Mechanics – Poisson Boltzmann and Surface Area) (Genheden and Ryde, 2015; Wang et al., 2001) as implemented in GMXPBSA 2.1 (Paissoni et al., 2015). Briefly, ligand/protein complexes were subjected to molecular dynamics simulations, and 100 frames were evenly extracted from the first 2 ns. The first 2 ns were chosen as the free energy estimate was intended as a post-docking scoring method, and not as an evaluation tool of the binding modes that vortioxetine converged into during the production runs. The first frame was extracted directly after the ligand restraints applied in the restrained equilibration phase were released, and the binding free energy is thus expected to reflect the binding mode found in the docking and not an MD-relaxed version of this binding mode. The trajectory was stripped of water, ions, and lipids and only the ligand and the two subunits within the ECD domain that surround the ligand along with the ligand itself were included in the calculations. APBS software (Baker et al., 2001) was used to solve the PB equation and for calculation of the nonpolar contribution to the solvation energy (on the basis of the solvent accessible surface area). Gromacs 5.0.2 and

Molecular Pharmacology Fast Forward. Published on September 26, 2018 as DOI: 10.1124/mol.118.113530
This article has not been copyedited and formatted. The final version may differ from this version.

the CHARMM36 force field (Best et al., 2012; Klauda et al., 2010) was used to calculate the van der Waals (vdW) and Coulomb energy contributions of the free ligand and protein, and the protein/ligand complex (Paissoni et al., 2015). The PB equation was solved using a nonlinear approximation with the boundary condition defined as *sdh* and a grid spacing of one with the temperature set to 310 K, ion concentrations to 0.2 M, and a protein dielectric constant of 2. Finally, the calculations were performed using the *multitrj* option in GMXPBSA to ensure same grid definitions in all calculations.

Molecular Pharmacology Fast Forward. Published on September 26, 2018 as DOI: 10.1124/mol.118.113530
This article has not been copyedited and formatted. The final version may differ from this version.

6. Results

Homology modeling of the h5-HT$_{3A}$ receptor structure — To enable computational studies of vortioxetine binding to the h5-HT$_{3A}$ receptor, we generated a three-dimensional molecular model of h5-HT$_{3A}$ using existing X-ray crystal structures of pLGICs and 5-HTBP constructs as templates (see *Materials and Methods* and *Supplemental Methods*) (Fig. 1). Vortioxetine acts as a functional antagonist at h5-HT$_{3A}$ by stabilizing the receptor in a closed channel state (Bang-Andersen et al., 2011). We, therefore, chose to model the h5-HT$_{3A}$ receptor in an inactive conformation; here defined as *i*) the channel adopting a conformation with gating residues obstructing ion passage as observed in closed-pore pLGIC structures (Dacosta and Baenziger, 2013; Sauguet et al., 2015) and *ii*) the orthosteric binding site adopting a conformation similar to structures of antagonist-bound pLGICs and 5-HTBP constructs (Kesters et al., 2013; Sander et al., 2010). We used multiple structures as templates to build this model because a single template did not exist that represented an inactive pLGIC conformation while being sufficiently homologous to the h5-HT$_{3A}$ receptor at the time of modeling. At the time of modeling, the closest homolog of h5-HT$_{3A}$ for which a high-resolution structure exists is the m5-HT$_{3A}$ receptor in the *apo* state (Hassaine et al., 2014). Human and mouse 5-HT$_{3A}$ receptors share 86% sequence identity, and the m5-HT$_{3A}$ structure is, therefore, in general, an excellent template for modeling of h5-HT$_{3A}$. However, the conformational state of the channel is unclear in the m5-HT$_{3A}$ structure due to the low resolution of the TMD region (Hassaine et al., 2014). Therefore, to model an inactive conformational state of h5-HT$_{3A}$, we combined the m5-HT$_{3A}$ structure with a structure of the human GABA$_A$ receptor (*Materials and Methods* and *Supplemental Methods*), which unambiguously is in a closed pore conformation (Miller

Molecular Pharmacology Fast Forward. Published on September 26, 2018 as DOI: 10.1124/mol.118.113530
This article has not been copyedited and formatted. The final version may differ from this version.

and Aricescu, 2014). The intracellular domain (ICD) formed by the 114-residue loops between the M3 and M4 membrane-spanning domains from each subunit is not resolved in the m5-HT_{3A} structure. Therefore, we did not model the ICD and instead replaced the M3-M4 loop in each h5-HT_{3A} subunit with a three amino acid artificial linker sequence (*Supplemental Methods*). Lastly, the conformation of the ECD loop regions that form the orthosteric binding sites were modeled using the reported X-ray crystal structure of granisetron-bound 5-HTBP (Kesters et al., 2013). The resulting h5-HT_{3A} model is shown in Fig. 1A and B. The orthosteric binding sites are located at the interfaces between subunits and formed by residues located in loops A-C on one subunit (denoted the principal subunit) and loops D-F on the neighboring subunit (denoted the complementary subunit) (Fig. 2A). In our model, loop C adopts an open conformation similar to the conformation observed for antagonist-bound ECD structures such as 5-HTBP in complex with setrons (Kesters et al., 2013; Price et al., 2016) as well as other antagonist-bound AChBP structures (Sander et al., 2010). Outside the binding site regions, the Cys-loop is in direct contact with the M2/M3 loop through hydrophobic interactions; a configuration predicted to be important for allosteric communication of conformational changes between the ECD and the transmembrane domain (TMD) (Jha et al., 2007). The narrowest diameter of the channel pore is 2.7 Å, which is in between the pore diameters of the template $GABA_A$ and m5-HT_{3A} receptor structures and is too narrow to allow ion passage (Mahler and Persson, 2012; Yang, 1990). The pore-lining residues all point into the channel pore, and the selectivity filter (Glu272) and the hydrophobic gate (Leu282) (Barnes et al., 2009) is closed.

Molecular Pharmacology Fast Forward. Published on September 26, 2018 as DOI: 10.1124/mol.118.113530
This article has not been copyedited and formatted. The final version may differ from this version.

Computational analysis of ligand binding to h5-HT$_{3A}$ – We initially evaluated the h5-HT$_{3A}$ receptor model by docking granisetron into the orthosteric site using an IFD protocol (*Materials and Methods*) and compared the resulting ligand-docking models with the existing structure of 5-HTBP in complex with granisetron. The resulting largest binding cluster of granisetron in the h5-HT$_{3A}$ model overlapped well with the binding mode observed in the 5-HTBP/granisetron structure (PDB ID: 2YME, Fig. 2B); thus suggesting that our h5-HT$_{3A}$ model and docking approach is suitable for exploration of potential bioactive binding modes in the orthosteric site. As the conformation of the orthosteric binding site in our h5-HT$_{3A}$ model is based on an antagonist-bound template, the binding site should be able to reproduce the granisetron binding mode found in a crystal structure of 5-HTBP (Kesters et al., 2013). We then docked vortioxetine into this validated model. We performed docking calculations in all five binding sites to improve the sampling of binding modes as each binding site is slightly different as no symmetry constraints were imposed during the modeling process. In total, 263 poses of vortioxetine were obtained from the five IFD calculations and clustered collectively according to their in-place conformation (*Materials and Methods*). Among these, we dismissed all clusters with average XP Gscores higher than -10 kcal/mol and/or clusters containing less than 6 poses. The XP Gscore is an empirical scoring function that seeks to estimate the ligand/protein binding affinity (Friesner et al., 2006). Six clusters remained and were considered as representing the potential bioactive binding mode (C2, C6, C8, C11, C13, and C30; Table 1). A representative orientation of vortioxetine in each of these six clusters is shown in Fig. 3A-F. Among these, the orientation and binding site interactions of vortioxetine differ in several aspects. First, different interaction partners are observed for the charged nitrogen

Molecular Pharmacology Fast Forward. Published on September 26, 2018 as DOI: 10.1124/mol.118.113530
This article has not been copyedited and formatted. The final version may differ from this version.

in the piperazine ring. In cluster C2, the charged nitrogen forms hydrogen bonds to the backbone carbonyls of Ser177 and Trp178 on loop B in addition to a cation/π interaction with Trp178. In cluster C6, the nitrogen is observed to form a salt bridge with Glu231 (loop C), whereas in cluster C8, C11, and C13, the nitrogen display cation/π interactions with Trp178 (loop B) and Tyr229 (loop C) and hydrogen bonding to Thr176 (loop B). Lastly, cluster C30 shows that the nitrogen atom in the piperazine ring is placed in the complementary subunit of the binding site where it forms a salt bridge to Asp64. Secondly, in all clusters one of the two aromatic rings in vortioxetine is located in the same sub-pocket at the "back" of the binding site in which one of the aromatic rings of vortioxetine is sandwiched between Tyr148 (loop E) and Trp85 (loop D) with further supporting interactions provided by Trp178 (loop B). In clusters C2, C6, and C8, the di-dimethylphenyl ring (phenyl A, Fig. 1C) is located in this sub-pocket, whereas in clusters C11, C13, and C30, it is the central phenyl (phenyl B, Fig. 1C). π/π stacking of either phenyl of vortioxetine to at least one of the three aromatic residues within this sub-pocket is observed in almost all docking poses. The location of the second phenyl ring of vortioxetine is less well-defined and can be found in one of three potential locations within the binding site. In clusters C2, C6, C13, and C30 the second phenyl ring is found close to loop A, B, and C and can interact with Tyr229 (loop C) and Thr176 (loop B). However, in C11 the second phenyl, in this case phenyl A, is located close to Ile66 and Val202 (loop F) of the complementary face, while in C8, phenyl B is located at the "top" of the binding site close to Y148 from loop E and Leu179 from loop B. It thus becomes clear that while vortioxetine forms interactions with the same aromatic residues either by cation/π, π/π, or

Molecular Pharmacology Fast Forward. Published on September 26, 2018 as DOI: 10.1124/mol.118.113530
This article has not been copyedited and formatted. The final version may differ from this version.

hydrophobic interactions, the binding clusters found in the docking calculations have distinct variations.

We further evaluated the binding clusters by performing MD simulations of each binding mode to determine the general stability of each binding mode and to estimate relative free energies of binding using the MM-PBSA approach (*Materials and Methods*). MM-PBSA is an efficient method for fast calculation of free energies of diverse molecular systems (Homeyer and Gohlke, 2012). For clusters C8 and C13, analysis of the RMSD progression in the MD trajectories showed the ligand remaining close to its initial conformation and position for the entire simulation period (Fig. 4C and E), suggesting these conformations represent possible stable binding modes. In contrast, the ligand changed conformation and position early during the simulations in cluster C2, C6, C11, and C30 (Fig. 4A, B, D, and F); at approximately 2 ns for C6, 10 ns for C2 and C11, and immediately for C30. Interestingly, for C6 and C11, the ligand converges on a conformation similar to those observed in the stable C8 and C13, respectively. C2 converged towards a unique conformation by shifting deeper into the binding site allowing the charged amine in the piperazine ring of vortioxetine to interact with Thr176 (loop B) (Fig. 4A). Furthermore, phenyl A rotates approximately 180°. The ligand in C30 does not change conformation during the MD simulation, but its position is shifted a few Ångström closer to the complementary subunit whereby improving electrostatic interactions with both Asp199 and Glu224 (loop F and C, respectively). We then used the MD trajectories to perform MM-PBSA calculations to estimate the free energy of binding for each cluster (*Materials and Methods*). The calculations were performed using the first 2 ns of the MD simulations to sample only the initial binding conformations. The resulting binding energies show

Molecular Pharmacology Fast Forward. Published on September 26, 2018 as DOI: 10.1124/mol.118.113530
This article has not been copyedited and formatted. The final version may differ from this version.

clusters C8, C11, and C13 to represent the strongest binding modes (Table 2). Considered together, the results of the MD simulations and the MM-PBSA calculations suggest that C8 and C13 represent the strongest and most stable binding mode of vortioxetine in h5-HT_{3A}.

Characterization of vortioxetine activity at h5-HT_{3A} receptors – Vortioxetine properties were characterized *in vitro* at recombinant h5-HT_{3A} receptors with the aim to establish a methodology for determination of effects of mutation of key binding site residues on vortioxetine affinity that would allow us to challenge the binding models. Previous work with recombinant h5-HT_{3A} receptors has shown vortioxetine to induce a rapidly desensitizing inward current with a peak response around 65% of that of 5-HT (Bang-Andersen et al., 2011). Using two-electrode voltage-clamp (TEVC) electrophysiology to measure recombinant h5-HT_{3A} currents in *Xenopus* oocytes (*Materials & methods*), we observed similar results with saturating concentrations of vortioxetine inducing inward currents with peak response of 54% relative to 5-HT and a 7-fold faster rate of desensitization (τ_{des}) for vortioxetine ($\tau_{des} = 7 \pm 4$ s; $n = 4$) compared to 5-HT ($\tau_{des} = 124 \pm 25$ s for 5-HT, $n = 4$) (Fig. 5B and 5C). Following wash-out of vortioxetine, a persistent inhibition of agonist-evoked currents was observed as the subsequent application of 5-HT was unable to induce responses, consistent with what has been previously reported (Fig. 5A) (Bang-Andersen et al., 2011; Dale et al., 2017). Thus, in the TEVC assay, the persistent vortioxetine inhibition of h5-HT_{3A} prevents multiple applications of different vortioxetine concentrations to the same oocyte that are practically required for concentration-response experiments for determination of ligand potency. Thus, for a higher throughput method of determining potency of 5-HT and inhibitory

Molecular Pharmacology Fast Forward. Published on September 26, 2018 as DOI: 10.1124/mol.118.113530
This article has not been copyedited and formatted. The final version may differ from this version.

potency (IC_{50}) of vortioxetine, we transiently expressed WT and mutant h5-HT_{3A} receptors in HEK-293 cells and used a micro plate-based functional assay that has been used extensively for 5-HT_3 receptor pharmacological characterization (*Materials and Methods* and *Supplemental Methods*) (Del Cadia et al., 2013; Lummis et al., 2011; Price et al., 2008; Price and Lummis, 2005; Sullivan et al., 2006; Thompson et al., 2006a). The assay is based on measurement of agonist-evoked changes in cell membrane potential by use of a fluorescent dye that is sensitive to the membrane field potential (Fitch et al., 2003). We evaluated the applicability of the assay by determining the concentration-response relationship for 5-HT (Fig. 5A) and concentration-inhibition relationships for two prototypical antagonists (granisetron and ondansetron) at WT h5-HT_{3A} (Supplemental Figure S2). The membrane potential assay yielded an EC_{50} for 5-HT of 191 nM (170-215 nM; n = 15) that are in close range of the EC_{50} value of 445 nM (255-685 nM; n = 8) determined from TEVC recordings (Fig. 6B-C). We obtained IC_{50} values of 3.3 nM (2.7-4.1 nM; n = 6) for granisetron and 0.87 nM (0.69-1.10 nM; n = 4) for ondansetron. These values are consistent with previously reported IC_{50} values for these compounds at h5-HT_{3A} receptors (Brady et al., 2001; Hope et al., 1996; Miyake et al., 1995); thus corroborating previous assessments of the usefulness of membrane potential assay for pharmacological characterization of recombinant 5-HT_3 receptors (Lummis and Thompson, 2013; Price and Lummis, 2005). We next used the membrane potential assay to determine the concentration-inhibition relationship of vortioxetine at 5-HT_{3A} (Fig. 6). When the cells were preincubated in increasing concentrations of vortioxetine, an IC_{50} of 19 nM (17-21 nM; n = 20) was found (Fig. 6E and 6F) which is similar to the IC_{50} of 12 nM for inhibition of h5-HT_{3A} activity in *Xenopus* oocytes as determined by Bang-Andersen *et al*. (2011) and

Molecular Pharmacology Fast Forward. Published on September 26, 2018 as DOI: 10.1124/mol.118.113530
This article has not been copyedited and formatted. The final version may differ from this version.

in HEK-293 cells by Dale *et al.* (2018). We also determined vortioxetine K_i from radioligand displacement experiments using the orthosteric 5-HT_3 ligand [^{3}H]-GR65630, and obtained a K_i of 22 nM (14-34 nM; $n = 4$) (Figure 6G) and conducted saturation binding experiments using [^{3}H]-vortioxetine to determine a K_d of 19 ± 6 nM (SEM; $n = 3$) (Fig. 6H). These values correspond well with the IC_{50} of vortioxetine determined in the membrane potential assay, which suggests that this assay can report affinity of vortioxetine for h5-HT_{3A} receptors. Furthermore, the highly persistent binding of vortioxetine to recombinant h5-HT_{3A} receptors observed in *Xenopus* oocytes suggest a very slow dissociation rate; i.e., that after extensive washout of vortioxetine from pre-incubated oocytes, all further application of 5-HT does not induce any current response to 5-HT. In the membrane potential assay which employs pre-incubation with vortioxetine before h5-HT_{3A} responses are evoked with 5-HT, such slow unbinding should make the IC_{50} of vortioxetine independent of 5-HT concentration. Indeed, using varying concentrations of 5-HT ranging from 1 to 300 μM generated identical IC_{50} curves (Fig. 6F). Thus, the membrane potential assay overall appears suitable for characterization of vortioxetine pharmacological properties at the h5-HT_{3A}.

Mutational analysis of binding site residues that are predicted critical for vortioxetine potency – To determine the potential contribution of binding site residues to vortioxetine affinity, we performed site-directed mutagenesis in the h5-HT_{3A} receptor and assessed the effect of single-point mutations on vortioxetine IC_{50} using the membrane potential assay. We selected eight amino acid positions around the orthosteric binding pocket for mutational analysis (Fig. 7A). The rationale for how mutation of these residues might allow us to discriminate between potential binding modes is outlined in Table 3. In

Molecular Pharmacology Fast Forward. Published on September 26, 2018 as DOI: 10.1124/mol.118.113530
This article has not been copyedited and formatted. The final version may differ from this version.

general, we substituted each position with one or more residues with different physicochemical properties from the WT residue so that the mutations could change potential interactions with vortioxetine. In total, we created 14 mutants (Table 4) that were individually expressed in HEK-293 cells and assessed for potential effects of mutation on overall receptor activity and 5-HT EC_{50} using the membrane potential assay (*Materials & Methods*). Four mutants (D64V, N123I, S177E, and E231I) did not show specific responses to 5-HT stimulation at concentrations up to 1 mM (Table 4). Thus, these mutations either disrupt receptor folding and assembly, surface expression, or function. In any case, the lack of activity in the membrane potential assay prevented characterization of the potential impact of the mutations on vortioxetine pharmacology. Therefore, these functionally inactive mutants were not studied further. Previous work has reported functional mutants of Asn123 (Ala and Asp) (Thompson et al., 2005) and Ser177 (Ala and Thr) (Thompson et al., 2005) in m5-HT_{3A}, and Glu231 in both h5-HT_{3A} and m5-HT_{3A} (Gln, Asp, and Ala) (Schreiter et al., 2003; Thompson et al., 2005), whereas mutants of Asp64 has not previously been tested according to the best of our knowledge.

The remaining ten mutants (covering five positions) were found to generate robust responses to 5-HT stimulation that allowed for determination of 5-HT EC_{50} (Table 4). Increases in 5-HT EC_{50} were observed for the V202A mutation and all substitutions at Thr176 and Asn123 (Table 4). These effects likely reflect that Thr176, Asn123, and V202A interact directly with 5-HT, and previous studies have observed similar shifts in 5-HT affinity upon mutations of Thr176 and Asn123 (Sullivan et al., 2006; Thompson et al., 2011). The remaining mutants displayed 5-HT EC_{50} within 2-fold range of WT. We then determined vortioxetine IC_{50} at all functional binding site mutants (Fig. 7 and Table 4).

The mutations T176V and V202A significantly increased vortioxetine IC_{50} by 5- and 11-fold, respectively, while the V202L mutation decreased the vortioxetine IC_{50} by 5-fold (Fig. 8 and Table 4). In contrast, all mutations of Ile66, Asn123, and Met223 produced less than 2-fold changes in vortioxetine IC_{50} (Fig. 8 and Table 4). These results suggest key contributions of the side chains of Thr176 and Val202 to vortioxetine binding, and no or limited contributions from Ile66, Asn123, and Met223.

Correlation of binding modes and mutant effects – We used the dataset from the mutational analysis as a final assessment of the potential of each binding mode cluster to represent the bioactive binding mode of vortioxetine in the h5-HT_{3A} receptor. The main observations that a bioactive binding mode should reconcile are: *i*) gain- or loss-of-potency upon change in bulk size of hydrophobic side chains of Val202 on loop F; *ii*) no or small effects upon change in bulk size of hydrophobic side chains at Ile66, and *iii*) the 5-fold loss-of-potency upon removal of the side chain hydrophilicity of T176. Overall, the orientations and positions of vortioxetine in binding cluster C2, C6, and C8 do not fit well with two of these observations. First, in these binding modes, the side chain of Val202 is located >6 Å from vortioxetine and displays no interactions with the ligand, which is inconsistent with the observations that vortioxetine potency is very sensitive to decrease (V202A) or subtle increase (V202L) in the bulk size of the side chain while maintaining hydrophobicity. Second, the C2, C6, and C8 binding modes predict phenyl A of vortioxetine to be located in a hydrophobic sub-pocket where it forms direct hydrophobic interactions with Ile66; an orientation that is inconsistent with the observed little or no effect of I66A and I66L mutations (Fig. 8).

Molecular Pharmacology Fast Forward. Published on September 26, 2018 as DOI: 10.1124/mol.118.113530
This article has not been copyedited and formatted. The final version may differ from this version.

The C11 binding mode overall fits well with the results from the mutational analysis. Vortioxetine is positioned sufficiently close to Val202 to form hydrophobic interactions with the side chain *via* phenyl A, which agrees with the observed effects of decreased potency upon substitution with the smaller Ala by the V202A mutation. The side chain of Ile66 is not in direct contact with vortioxetine in the stabilized conformation found *via* MD simulations; thus being consistent with the lack of effect of the I66A and I66L mutations. The impact of the T176V mutation on vortioxetine potency is also compatible with this binding mode as C11 predicts the presence of a hydrogen bond between the ligand piperazine secondary amine and the Thr176 side chain hydroxyl group. T176V substitutes this hydroxyl for methyl and thus disrupts any hydrogen bond capacity of this side chain; consistent with the observed 6-fold decrease in potency for the T176V mutant.

In C13, which was stable during MD simulations, Val202 is making hydrophobic contacts to phenyl A, and Ile66 is not in close contact with vortioxetine; thus consistent with the mutational results for these two residues. However, C13 predict no ligand interaction with the side chain of Thr176 in the IFD data, in which the hydroxyl group is pointing away from the ligand. However, the MD simulations of C13 show that the side chain of Thr176 reorient such that hydrogen bonds can form between the side chain hydroxyl and the secondary amine in the piperazine ring of vortioxetine and loss of this interaction may underlie the effect of the T176V mutation.

In C30, the side chain of Ile66 is around 4 Å from the piperazine ring, which is sufficiently distant to explain the lack of effect of Ile66 mutations that alter the bulk size of the side chain. However, Val202 is approximately 5 Å away from the ligand, which is not compatible with the substantial effects of subtle changes in the bulk size of the side

chain. Moreover, on the opposite side of the binding pocket, the side chain of Thr176 is also more than 5 Å away from the ligand, which cannot explain the T176V effect.

In summary, the binding modes of vortioxetine observed in the C2, C6, C8, and C30 docking clusters are not compatible with the results from the mutational analysis. Combined with the results of the MD simulations and binding energy analysis, we exclude these as potential bioactive binding modes. C11 and C13 display compatibility with all mutational observations when including data from both IFD calculations and MD simulations and may thus represent bioactive conformations of vortioxetine *in vivo*. During the MD simulations of C11, vortioxetine assumed a conformation that is highly similar to the conformation in C13. It is noteworthy that these binding modes then only differ by a 180° rotation of phenyl A such that the *ortho*-methyl group is pointing in opposing directions. Thus, we suggest that C11 and C13 collectively represent the binding modes of vortioxetine in the h5-HT_{3A} receptor in which vortioxetine binds with some flexibility as it can bind to the receptor with the aromatic ring A in two orientations.

Molecular Pharmacology Fast Forward. Published on September 26, 2018 as DOI: 10.1124/mol.118.113530
This article has not been copyedited and formatted. The final version may differ from this version.

7. Discussion

Our model of the vortioxetine binding mode at the h5-HT_{3A} receptor provides insight into the molecular basis for the potentially unique mode of action of vortioxetine at the 5-HT_3 receptor class. In the absence of a high-resolution structure of the h5-HT_{3A} receptor, we used homology modeling to create a structural model of the receptor in an inactive state. Recently, structures of antagonist-bound eukaryotic pLGIC receptors have become available in the form of cryoEM structures of a zebra fish GlyR (Du et al., 2015; Huang et al., 2015). Furthermore, a crystal structure of a desensitized nAChR (Morales-Perez et al., 2016) and a cryoEM structure of a pre-activated m5-HT_{3A} receptor (Basak et al., 2018) have recently been published. In comparison to these structures, we find that the structures of the GlyR ECDs are very similar to our model. The single major difference is the structure of the F loop region that in our h5-HT_{3A} model and the m5-HT_{3A} crystal structure (Hassaine et al., 2014) contains a short α-helical segment, which the GlyR structures do not. The Val202 residue important for vortioxetine binding is located in the F loop; however, outside the helical segment in a region where our model and GlyR are highly similar. Additionally, our h5-HT_{3A} model is highly similar to the pre-activated conformation of m5-HT_{3A} (Basak et al., 2018). These observations suggest that our model is a good representative for the inactive conformation of the h5-HT_{3A} receptor. In contrast, the conformation of h5-HT_{3A} in our model is considerably less similar to the desensitized conformation of nAChR (Morales-Perez et al., 2016). As vortioxetine produces a brief agonist response in 5-HT_{3A} followed by fast and prolonged desensitization, it is possible that vortioxetine binds with strongest affinity to the desensitized state. It would therefore be highly relevant in future work to investigate if our proposed vortioxetine binding mode is changed in an h5$HT3_A$

Molecular Pharmacology Fast Forward. Published on September 26, 2018 as DOI: 10.1124/mol.118.113530
This article has not been copyedited and formatted. The final version may differ from this version.

model in the desensitized state. However, by the overall high degree of structural similarity to the pre-activated m5-HT_{3A}, and in the ECD regions which harbor the orthosteric binding sites between our model and antagonist-bound GlyRs, we consider our present model a valid template for the ligand docking of vortioxetine.

Our ligand docking procedure yielded six possible binding modes of vortioxetine in the orthosteric binding site of the h5-HT_{3A} receptor. Following a further assessment by MD simulations and binding free energy calculations, these six were narrowed down to three stable binding modes as candidates for the receptor-bound bioactive conformation of vortioxetine. We further evaluated these binding modes by mutagenesis of selected amino acid residues in the binding pocket. The observed effects of mutations on vortioxetine potency could only be fully reconciled with the highly similar C11 and C13 binding modes (Fig. 8). We, therefore, propose C11 and C13 as the bioactive binding modes. The resulting model of vortioxetine binding in the h5-HT_{3A} receptor provides a framework to understand the molecular basis for the differential mechanism of action of vortioxetine at 5-HT_{3A} compared with other 5-HT_3 orthosteric ligands. As other pLGICs, the h5-HT_{3A} orthosteric binding pocket contains an 'aromatic box' structural motif formed by Trp, Tyr, and Phe residues on loop A, B, C, and D (Fig. 8; Trp85, Phe221, Tyr229, and Trp178 in h5-HT_{3A}) (Beene et al., 2002a; Beene et al., 2002b; Thompson et al., 2010; Xiu et al., 2009). The role of these residues are extensively studied in the 5-HT_3 receptor (Beene et al., 2002a; Beene et al., 2002b; Beene et al., 2004; Price et al., 2008), and multiple models exist for their role in binding of setrons and agonists. Early models and more recently also X-ray structures of 5-HTBP in complex with setrons collectively show three main factors necessary for setron binding and effect: *i*) hydrogen bonds and cat/π interactions with Trp178 in the

Molecular Pharmacology Fast Forward. Published on September 26, 2018 as DOI: 10.1124/mol.118.113530
This article has not been copyedited and formatted. The final version may differ from this version.

aromatic box (Kesters et al., 2013; Lochner and Thompson, 2016; Price et al., 2016), *ii*) cation/π and/or π/π interactions with Tyr136, Tyr138, Tyr148, and Arg87 (Beene et al., 2004; Joshi et al., 2006; Thompson et al., 2005; Thompson et al., 2014; Yan and White, 2005), and *iii*) setron occupation of a subsite beyond Arg87 near loop D and F (Fig. 8) (Kesters et al., 2013; Lochner and Thompson, 2016; Price et al., 2016). In our model, vortioxetine appears to interact with key motifs of the aromatic box in a similar manner, but also displays interactions that are distinct from setrons. A key similarity is the charged nitrogen on the piperazine ring which is located in the center of the box and forms cation/π interactions to Trp178 and Tyr148 (Fig. 8). However, unlike setrons, vortioxetine does not interact with Tyr136, Tyr138, and Arg87 and does not occupy the sub-pocket beyond Arg87 (Fig. 8). Thus, the interaction pattern of vortioxetine is distinct from setrons.

In contrast to setrons, at saturating concentrations, vortioxetine also displays agonist activity at 5-HT_{3A}. As for setrons, agonist binding has been shown to require hydrogen bonding and cation/π interactions with Trp178 (Beene et al., 2002b; Price et al., 2016), suggesting this interaction to be a common denominator for ligand binding in 5-HT_3 receptors. Unlike the setrons, however, agonists interact with the 5-HTBP equivalent of Tyr148 within the complementary face and are not able to reach as far as Arg87 in loop D (Thompson et al., 2006a). Also, agonists interact with residues from loop E as well as loop D deep within the orthosteric binding pocket (Fig. 8B). Interestingly, in our model, vortioxetine does not interact with either of these two subsites but does interact with a subsite located at loop E closer to the membrane. This unique interaction pattern of vortioxetine could underlie its distinct functional profile. In this respect, it is interesting to note that previous studies have shown Trp85 from loop D (Spier and Lummis, 2000) as

Molecular Pharmacology Fast Forward. Published on September 26, 2018 as DOI: 10.1124/mol.118.113530
This article has not been copyedited and formatted. The final version may differ from this version.

well as Tyr138 and Tyr148 from loop E (Beene et al., 2004; Price and Lummis, 2004) to be necessary to produce an agonist effect and vortioxetine interacts extensively with both Trp85 and Tyr148 in our model.

The antidepressant effect of vortioxetine involves its highly potent inhibition of SERT (Andersen et al., 2009; Bang-Andersen et al., 2011). We have previously reported a model of vortioxetine bound in human SERT (hSERT) (Andersen et al., 2015). Key insights into the role of functional groups of vortioxetine in binding hSERT and h5-HT_{3A} are of potential interest for future drug design of multimodal drugs targeting these serotonergic proteins. First, in both hSERT and h5-HT_{3A}, the interactions of the positively charged nitrogen in the piperazine ring mimic the interactions with the primary amine of 5-HT. Specifically, the piperazine nitrogen forms an important salt bridge to Asp98 in hSERT, and make hydrogen bond and cation/π interactions to Thr176 and Trp178, respectively, in h5-HT_{3A}. A contrasting feature is the overall role of the two phenyl rings of vortioxetine for binding at hSERT and h5-HT_{3A}. At h5-HT_{3A}, the phenyl rings make several π/π and cation/π interactions, in particular to residues in the aromatic box, whereas in hSERT, hydrophobicity of the phenyl rings rather than the aromaticity is most important for binding (Andersen et al., 2015).

In summary, we have created and validated a model of the bioactive conformation of vortioxetine in the h5-HT_{3A} receptor that provides new insight into the binding of a novel multimodal serotonergic drug. The binding pattern of vortioxetine mimics some aspects of both setron and 5-HT binding but also displays binding interactions not previously described to be important for binding of either setrons or 5-HT. As the mechanism of vortioxetine differs from classical 5-HT_{3A} orthosteric ligands with inhibitory activity such

as the setrons, our results may be an important first step towards understanding the molecular basis underlying the unique properties of vortioxetine. Specifically, this will include understanding the molecular determinants for how vortioxetine binding induces a brief agonistic response followed by a rapid transition into a desensitized state from which vortioxetine has an extremely slow unbinding rate. Finally, our results provide guidance in efforts to develop multimodal drugs with tailored activity across the spectrum of serotonergic receptors.

8. Authorship Contributions

Participated in research design: Ladefoged, Munro, Balle, Bang-Andersen, Schiøtt, Lummis, and Kristensen.

Conducted experiments: Ladefoged, Munro, and Pedersen.

Contributed new reagents or analytic tools: Lummis, Bang-Andersen.

Performed data analysis: Ladefoged, Munro, and Kristensen.

Wrote or contributed to the writing of the manuscript: Ladefoged, Munro, Balle, Bang-Andersen, Schiøtt, and Kristensen.

9. References

Alix K, Khatri S, Mosier PD, Casterlow S, Yan D, Nyce HL, White MM, Schulte MK and Dukat M (2016) Superagonist, Full Agonist, Partial Agonist, and Antagonist Actions of Arylguanidines at 5-Hydroxytryptamine-3 (5-HT3) Subunit A Receptors. *ACS Chem Neurosci* **7**(11): 1565-1574.

Althoff T, Hibbs RE, Banerjee S and Gouaux E (2014) X-ray structures of GluCl in apo states reveal a gating mechanism of Cys-loop receptors. *Nature* **512**(7514): 333-337.

Andersen J, Kristensen AS, Bang-Andersen B and Stromgaard K (2009) Recent advances in the understanding of the interaction of antidepressant drugs with serotonin and norepinephrine transporters. *Chem Commun (Camb)*(25): 3677-3692.

Andersen J, Ladefoged LK, Wang DY, Kristensen TNB, Bang-Andersen B, Kristensen AS, Schiott B and Stromgaard K (2015) Binding of the Multimodal Antidepressant Drug Vortioxetine to the Human Serotonin Transporter. *ACS Chem Neurosci* **6**(11): 1892-1900.

Andersen N, Corradi J, Sine SM and Bouzat C (2013) Stoichiometry for activation of neuronal alpha 7 nicotinic receptors. *Proceedings of the National Academy of Sciences of the United States of America* **110**(51): 20819-20824.

Baker NA, Sept D, Joseph S, Holst MJ and McCammon JA (2001) Electrostatics of nanosystems: Application to microtubules and the ribosome. *Proceedings of the National Academy of Sciences of the United States of America* **98**(18): 10037-10041.

Bang-Andersen B, Ruhland T, Jorgensen M, Smith G, Frederiksen K, Jensen KG, Zhong H, Nielsen SM, Hogg S, Mork A and Stensbol TB (2011) Discovery of 1-[2-(2,4-dimethylphenylsulfanyl)phenyl]piperazine (Lu AA21004): a novel multimodal compound for the treatment of major depressive disorder. *J Med Chem* **54**(9): 3206-3221.

Barbosa AJM, De Rienzo F, Ramos MJ and Menziani MC (2010) Computational analysis of ligand recognition sites of homo- and heteropentameric 5-HT3 receptors. *Eur J Med Chem* **45**(11): 4746-4760.

Barnes NM, Hales TG, Lummis SC and Peters JA (2009) The 5-HT3 receptor--the relationship between structure and function. *Neuropharmacology* **56**(1): 273-284.

Basak S, Gicheru Y, Samanta A, Molugu SK, Huang W, la de Fuente M, Hughes T, Taylor DJ, Nieman MT, Moiseenkova-Bell V and Chakrapani S (2018) Cryo-EM structure of 5-HT3A receptor in its resting conformation. *Nat Commun* **9** (1):514

Beene DL, Brandt GS, Lester HA and Dougherty DA (2002a) Comparison of the cation-pi interaction at the agonist binding-sites of the nicotinic-acetylcholine receptor and the 5-hydroxytryptamine-3 receptor. *Biophys J* **82**(1): 257a-257a.

Beene DL, Brandt GS, Zhong WG, Zacharias NM, Lester HA and Dougherty DA (2002b) Cation-pi interactions in ligand recognition by serotonergic (5-HT3A) and nicotinic acetylcholine receptors: The anomalous binding properties of nicotine. *Biochemistry* **41**(32): 10262-10269.

Beene DL, Price KL, Lester HA, Dougherty DA and Lummis SCR (2004) Tyrosine residues that control binding and Gating in the 5-hydroxytryptamine(3) receptor revealed by unnatural amino acid mutagenesis. *J Neurosci* **24**(41): 9097-9104.

Berger M, Gray JA and Roth BL (2009) The expanded biology of serotonin. *Annual review of medicine* **60**: 355-366.

Best RB, Zhu X, Shim J, Lopes PEM, Mittal J, Feig M and MacKerell AD (2012) Optimization of the Additive CHARMM All-Atom Protein Force Field Targeting Improved Sampling of the Backbone phi, psi and Side-Chain chi(1) and chi(2) Dihedral Angles. *J Chem Theory Comput* **8**(9): 3257-3273.

Brady CA, Stanford IM, Ali I, Lin L, Williams JM, Dubin AE, Hope AG and Barnes NM (2001) Pharmacological comparison of human homomeric 5-HT3A receptors versus heteromeric 5-HT3A/3B receptors. *Neuropharmacology* **41**(2): 282-284.

Brejc K, van Dijk WJ, Klaassen RV, Schuurmans M, van Der Oost J, Smit AB and Sixma TK (2001) Crystal structure of an ACh-binding protein reveals the ligand-binding domain of nicotinic receptors. *Nature* **411**(6835): 269-276.

Bulacu M, Goga N, Zhao W, Rossi G, Monticelli L, Periole X, Tieleman DP and Marrink SJ (2013) Improved Angle Potentials for Coarse-Grained Molecular Dynamics Simulations. *J Chem Theory Comput* **9**(8): 3282-3292.

Cheng Y and Prusoff WH (1973) Relationship between the inhibition constant (K1) and the concentration of inhibitor which causes 50 per cent inhibition (I50) of an enzymatic reaction. *Biochemical pharmacology* **22**(23): 3099-3108.

Corradi J, Gumilar F and Bouzat C (2009) Single-Channel Kinetic Analysis for Activation and Desensitization of Homomeric 5-HT(3)A Receptors. *Biophys J* **97**(5): 1335-1345.

Dacosta CJB and Baenziger JE (2013) Gating of Pentameric Ligand-Gated Ion Channels: Structural Insights and Ambiguities. *Structure* **21**(8): 1271-1283.

Dale E, Grunnet M, Pehrson AL, Frederiksen K, Larsen PH, Nielsen J, Stensbol TB, Ebert B, Yin HL, Lu DG, Liu HQ, Jensen TN, Yang CR and Sanchez C (2018) The multimodal antidepressant vortioxetine may facilitate pyramidal cell firing by inhibition of 5-HT3 receptor expressing interneurons: An in vitro study in rat hippocampus slices. *Brain research* **1689**: 1-11.

de Jong DH, Singh G, Bennett WFD, Arnarez C, Wassenaar TA, Schafer LV, Periole X, Tieleman DP and Marrink SJ (2013) Improved Parameters for the Martini Coarse-Grained Protein Force Field. *J Chem Theory Comput* **9**(1): 687-697.

Del Cadia M, De Rienzo F, Weston DA, Thompson AJ, Menziani MC and Lummis SC (2013) Exploring a potential palonosetron allosteric binding site in the 5-HT(3) receptor. *Bioorg Med Chem* **21**(23): 7523-7528.

Du J, Lu W, Wu SP, Cheng YF and Gouaux E (2015) Glycine receptor mechanism elucidated by electron cryo-microscopy. *Nature* **526**(7572): 224-229.

Fitch RW, Xiao Y, Kellar KJ and Daly JW (2003) Membrane potential fluorescence: a rapid and highly sensitive assay for nicotinic receptor channel function. *Proceedings of the National Academy of Sciences of the United States of America* **100**(8): 4909-4914.

Friesner RA, Banks JL, Murphy RB, Halgren TA, Klicic JJ, Mainz DT, Repasky MP, Knoll EH, Shelley M, Perry JK, Shaw DE, Francis P and Shenkin PS (2004) Glide: A new approach for rapid, accurate docking and scoring. 1. Method and assessment of docking accuracy. *J Med Chem* **47**(7): 1739-1749.

Friesner RA, Murphy RB, Repasky MP, Frye LL, Greenwood JR, Halgren TA, Sanschagrin PC and Mainz DT (2006) Extra precision glide: Docking and scoring

incorporating a model of hydrophobic enclosure for protein-ligand complexes. *J Med Chem* **49**(21): 6177-6196.

Genheden S and Ryde U (2015) The MM/PBSA and MM/GBSA methods to estimate ligand-binding affinities. *Expert Opin Drug Dis* **10**(5): 449-461.

Hassaine G, Deluz C, Grasso L, Wyss R, Tol MB, Hovius R, Graff A, Stahlberg H, Tomizaki T, Desmyter A, Moreau C, Li XD, Poitevin F, Vogel H and Nury H (2014) X-ray structure of the mouse serotonin 5-HT3 receptor. *Nature* **512**(7514): 276-281.

Hibbs RE and Gouaux E (2011a) Principles of activation and permeation in an anion-selective Cys-loop receptor. *Nature* **474**(7349): 54-60.

Homeyer N and Gohlke H (2012) Free Energy Calculations by the Molecular Mechanics Poisson-Boltzmann Surface Area Method. *Molecular informatics* **31**(2): 114-122.

Hope AG, Peters JA, Brown AM, Lambert JJ and Blackburn TP (1996) Characterization of a human 5-hydroxytryptamine3 receptor type A (h5-HT3R-AS) subunit stably expressed in HEK 293 cells. *British journal of pharmacology* **118**(5): 1237-1245.

Huang X, Chen H, Michelsen K, Schneider S and Shaffer PL (2015) Crystal structure of human glycine receptor-alpha 3 bound to antagonist strychnine. *Nature* **526**(7572): 277-280.

Huang X, Chen H and Shaffer PL (2017) Crystal Structures of Human GlyR alpha 3 Bound to Ivermectin. *Structure* **25**(6): 945- 950.

Jespersen T, Grunnet M, Angelo K, Klaerke DA and Olesen SP (2002) Dual-function vector for protein expression in both mammalian cells and Xenopus laevis oocytes. *Biotechniques* **32**(3): 536-538, 540.

Jha A, Cadugan DJ, Purohit P and Auerbach A (2007) Acetylcholine receptor gating at extracellular transmembrane domain interface: the Cys-loop and M2-M3 linker. *J Gen Physiol* **130**(6): 547-558.

Joshi PR, Suryanarayanan A, Hazai E, Schulte MK, Maksay G and Bikadi Z (2006) Interactions of Granisetron with an agonist-free 5-HT3A receptor model. *Biochemistry* **45**(4): 1099-1105.

Joshi PR, Suryanarayanan A and Schulte MK (2004) A vertical flow chamber for Xenopus oocyte electrophysiology and automated drug screening. *Journal of neuroscience methods* **132**(1): 69-79.

Kesters D, Thompson AJ, Brams M, van Elk R, Spurny R, Geitmann M, Villalgordo JM, Guskov A, Danielson UH, Lummis SC, Smit AB and Ulens C (2013) Structural basis of ligand recognition in 5-HT3 receptors. *EMBO Rep* **14**(1): 49-56.

Klauda JB, Venable RM, Freites JA, O'Connor JW, Tobias DJ, Mondragon-Ramirez C, Vorobyov I, MacKerell AD and Pastor RW (2010) Update of the CHARMM All-Atom Additive Force Field for Lipids: Validation on Six Lipid Types. *J Phys Chem B* **114**(23): 7830-7843.

Lochner M and Thompson AJ (2016) The muscarinic antagonists scopolamine and atropine are competitive antagonists at 5-HT3 receptors. *Neuropharmacology* **108**: 220-228.

Lummis SC (2012) 5-HT(3) receptors. *J Biol Chem* **287**(48): 40239-40245.

Lummis SC and Thompson AJ (2013) Agonists and antagonists induce different palonosetron dissociation rates in 5-HT(3)A and 5-HT(3)AB receptors. *Neuropharmacology* **73**: 241-246.

Lummis SC, Thompson AJ, Bencherif M and Lester HA (2011) Varenicline is a potent agonist of the human 5-hydroxytryptamine3 receptor. *J Pharmacol Exp Ther* **339**(1): 125-131.

Mahableshwarkar AR, Zajecka J, Jacobson W, Chen Y and Keefe RS (2015) A Randomized, Placebo-Controlled, Active-Reference, Double-Blind, Flexible-Dose Study of the Efficacy of Vortioxetine on Cognitive Function in Major Depressive Disorder. *Neuropsychopharmacology* **40**(8): 2025-2037.

Mahler J and Persson I (2012) A study of the hydration of the alkali metal ions in aqueous solution. *Inorg Chem* **51**(1): 425-438.

McIntyre RS, Florea I, Tonnoir B, Loft H, Lam RW and Christensen MC (2017) Efficacy of Vortioxetine on Cognitive Functioning in Working Patients With Major Depressive Disorder. *The Journal of clinical psychiatry* **78**(1): 115-121.

McIntyre RS, Lophaven S and Olsen CK (2014) A randomized, double-blind, placebo-controlled study of vortioxetine on cognitive function in depressed adults. *Int J Neuropsychopharmacol* **17**(10): 1557-1567.

Miller PS and Aricescu AR (2014) Crystal structure of a human GABA(A) receptor. *Nature* **512**(7514): 270-275.

Miller PS and Smart TG (2010) Binding, activation and modulation of Cys-loop receptors. *Trends Pharmacol Sci* **31**(4): 161-174.

Miyake A, Mochizuki S, Takemoto Y and Akuzawa S (1995) Molecular cloning of human 5-hydroxytryptamine3 receptor: heterogeneity in distribution and function among species. *Mol Pharmacol* **48**(3): 407-416.

Morales-Perez CL, Noviello CM and Hibbs RE (2016) X-ray structure of the human α4β2 nicotinic receptor. *Nature* **538**(7625): 411-415.

Mork A, Montezinho LP, Miller S, Trippodi-Murphy C, Plath N, Li Y, Gulinello M and Sanchez C (2013) Vortioxetine (Lu AA21004), a novel multimodal antidepressant, enhances memory in rats. *Pharmacology, biochemistry, and behavior* **105**: 41-50.

Nemecz A, Prevost MS, Menny A and Corringer PJ (2016) Emerging Molecular Mechanisms of Signal Transduction in Pentameric Ligand-Gated Ion Channels. *Neuron* **90**(3): 452-470.

Nys M, Kesters D and Ulens C (2013) Structural insights into Cys-loop receptor function and ligand recognition. *Biochem Pharmacol* **86**(8): 1042-1053.

Paissoni C, Spiliotopoulos D, Musco G and Spitaleri A (2015) GMXPBSA 2.1: A GROMACS tool to perform MM/PBSA and computational alanine scanning. *Comput Phys Commun* **186**(Supplement C): 105-107.

Poulsen MH, Lucas S, Bach TB, Barslund AF, Wenzler C, Jensen CB, Kristensen AS and Stromgaard K (2013) Structure-activity relationship studies of argiotoxins: selective and potent inhibitors of ionotropic glutamate receptors. *Journal of medicinal chemistry* **56**(3): 1171-1181.

Price KL, Bower KS, Thompson AJ, Lester HA, Dougherty DA and Lummis SCR (2008) A hydrogen bond in loop a is critical for the binding and function of the 5-HT3 receptor. *Biochemistry* **47**(24): 6370-6377.

Price KL, Lillestol RK, Ulens C and Lummis SC (2015) Varenicline Interactions at the 5-HT3 Receptor Ligand Binding Site are Revealed by 5-HTBP. *ACS Chem Neurosci* **6**(7): 1151-1157.

Price KL, Lillestol RK, Ulens C and Lummis SCR (2016) Palonosetron-5-HT3 Receptor Interactions As Shown by a Binding Protein Cocrystal Structure. *ACS Chem Neurosci* **7**(12): 1641-1646.

Price KL and Lummis SC (2005) FlexStation examination of 5-HT3 receptor function using Ca^{2+} - and membrane potential-sensitive dyes: advantages and potential problems. *J Neurosci Methods* **149**(2): 172-177.

Price KL and Lummis SCR (2004) The role of tyrosine residues in the extracellular domain of the 5-hydroxytryptamine(3) receptor. *J Biol Chem* **279**(22): 23294-23301.

Rayes D, De Rosa MJ, Sine SM and Bouzat C (2009) Number and Locations of Agonist Binding Sites Required to Activate Homomeric Cys-Loop Receptors. *J Neurosci* **29**(18): 6022-6032.

Riga MS, Sanchez C, Celada P and Artigas F (2016) Involvement of 5-HT3 receptors in the action of vortioxetine in rat brain: Focus on glutamatergic and GABAergic neurotransmission. *Neuropharmacology* **108**: 73-81.

Robertson DW, Lacefield WB, Bloomquist W, Pfeifer W, Simon RL and Cohen ML (1992) Zatosetron, a potent, selective, and long-acting 5HT3 receptor antagonist: synthesis and structure-activity relationships. *J Med Chem* **35**(2): 310-319.

Ruepp MD, Wei H, Leuenberger M, Lochner M and Thompson AJ (2017) The binding orientations of structurally-related ligands can differ; A cautionary note. *Neuropharmacology* **119**: 48-61.

Sali A and Blundell TL (1993) Comparative Protein Modeling by Satisfaction of Spatial Restraints. *Journal of molecular biology* **234**(3): 779-815.

Sanchez C, Asin KE and Artigas F (2015) Vortioxetine, a novel antidepressant with multimodal activity: review of preclinical and clinical data. *Pharmacol Ther* **145**: 43-57.

Sander T, Bruun AT and Balle T (2010) Docking to flexible nicotinic acetylcholine receptors: A validation study using the acetylcholine binding protein. *J Mol Graph Model* **29**(3): 415-424.

Sauguet L, Shahsavar A and Delarue M (2015) Crystallographic studies of pharmacological sites in pentameric ligand-gated ion channels. *Biochimica et biophysica acta* **1850**(3): 511-523.

Schreiter C, Hovius R, Costioli M, Pick H, Kellenberger S, Schild L and Vogel H (2003) Characterization of the ligand-binding site of the serotonin 5-HT3 receptor - The role of glutamate residues 97, 224, and 235. *J Biol Chem* **278**(25): 22709-22716.

Sherman W, Day T, Jacobson MP, Friesner RA and Farid R (2006) Novel procedure for modeling ligand/receptor induced fit effects. *J Med Chem* **49**(2): 534-553.

Smit AB, Syed NI, Schaap D, van Minnen J, Klumperman J, Kits KS, Lodder H, van der Schors RC, van Elk R, Sorgedrager B, Brejc K, Sixma TK and Geraerts WPM (2001) A glia-derived acetylcholine-binding protein that modulates synaptic transmission. *Nature* **411**(6835): 261-268.

Spier AD and Lummis SCR (2000) The role of tryptophan residues in the 5-hydroxytryptamines receptor ligand binding domain. *J Biol Chem* **275**(8): 5620-5625.

Sullivan NL, Thompson AJ, Price KL and Lummis SC (2006) Defining the roles of Asn-128, Glu-129 and Phe-130 in loop A of the 5-HT3 receptor. *Mol Membr Biol* **23**(5): 442-451.

Thompson AJ, Duke RK and Lummis SC (2011) Binding sites for bilobalide, diltiazem, ginkgolide, and picrotoxinin at the 5-HT3 receptor. *Mol Pharmacol* **80**(1): 183-190.

Thompson AJ, Lester HA and Lummis SCR (2010) The structural basis of function in Cys-loop receptors. *Q Rev Biophys* **43**(4): 449-499.

Thompson AJ, Padgett CL and Lummis SCR (2006a) Mutagenesis and molecular modeling reveal the importance of the 5-HT3 receptor F-loop. *J Biol Chem* **281**(24): 16576-16582.

Thompson AJ, Price KL, Reeves DC, Chan SL, Chau PL and Lummis SCR (2005) Locating an antagonist in the 5-HT3 receptor binding site using modeling and radioligand binding. *J Biol Chem* **280**(21): 20476-20482.

Thompson AJ, Sullivan NL and Lummis SC (2006b) Characterization of 5-HT3 receptor mutations identified in schizophrenic patients. *J Mol Neurosci* **30**(3): 273-281.

Thompson AJ, Verheij MHP, Verbeek J, Windhorst AD, de Esch IJP and Lummis SCR (2014) The binding characteristics and orientation of a novel radioligand with distinct properties at 5-HT(3)A and 5-HT(3)AB receptors. *Neuropharmacology* **86**: 378-388.

Unwin N (2005) Refined structure of the nicotinic acetylcholine receptor at 4 angstrom resolution. *Journal of molecular biology* **346**(4): 967-989.

Unwin N and Fujiyoshi Y (2012) Gating Movement of Acetylcholine Receptor Caught by Plunge-Freezing. *Journal of molecular biology* **422**(5): 617-634.

Wang JM, Morin P, Wang W and Kollman PA (2001) Use of MM-PBSA in reproducing the binding free energies to HIV-1 RT of TIBO derivatives and predicting the binding mode to HIV-1 RT of efavirenz by docking and MM-PBSA. *J Am Chem Soc* **123**(22): 5221-5230.

Xiu X, Puskar NL, Shanata JA, Lester HA and Dougherty DA (2009) Nicotine binding to brain receptors requires a strong cation-pi interaction. *Nature* **458**(7237): 534-537.

Yan D and White MM (2005) Spatial orientation of the antagonist granisetron in the ligand-binding site of the 5-HT3 receptor. *Mol Pharmacol* **68**(2): 365-371.

Yang J (1990) Ion permeation through 5-hydroxytryptamine-gated channels in neuroblastoma N18 cells. *J Gen Physiol* **96**(6): 1177-1198.

Zuber B and Unwin N (2013) Structure and superorganization of acetylcholine receptor-rapsyn complexes. *Proc Natl Acad Sci U S A* **110**(26): 10622-10627.

Molecular Pharmacology Fast Forward. Published on September 26, 2018 as DOI: 10.1124/mol.118.113530
This article has not been copyedited and formatted. The final version may differ from this version.

10. Footnotes

This work was supported by the Danish Council of Independent Research for Medical Sciences [grant number DFF-404-00309], the Lundbeck Foundation [grant number 2017-1655 and 2012-12453], and the Carlsberg Foundation. Computations were made possible through allocations at the Centre for Scientific Computing, Arhus (SCS-Aa). Disclosure: Dr. Benny Bang-Andersen is an employee of H. Lundbeck A/S.

Molecular Pharmacology Fast Forward. Published on September 26, 2018 as DOI: 10.1124/mol.118.113530
This article has not been copyedited and formatted. The final version may differ from this version.

11. Figure Legends

Figure 1. Structural model of the h5-HT_{3A} receptor and chemical structure of vortioxetine. ***A-B.*** Side (*A*) and top (*B*) views of ribbon representations of the h5-HT_{3A} receptor structure created by homology modeling. Each subunit in the pentameric complex is colored individually. Brackets indicate the location of the extracellular (ECD) and transmembrane (TMD) domains. ***C.*** Chemical structure of vortioxetine with an indication of the A and B ring nomenclature.

Figure 2. Granisetron docking in the orthosteric binding site of the model h5-HT_{3A} receptor structure. ***A.*** Ribbon representation of the orthosteric binding site in the h5-HT_{3A} receptor model at the subunit interface and is formed by loops A to C in the principal subunit and loops D to F in the complementary subunit. ***B.*** Structure of granisetron (*cyan*) docked in the h5-HT_{3A} receptor model overlayed with the experimentally determined structure of granisetron in complex with 5-HTBP (*blue*) (PDB ID: 2YME). Key principal and complimentary subunit residues are colored in *white* and *gray*, respectively. Residue numberings refer to the h5-HT_{3A} sequence.

Figure 3. Potential binding modes of vortioxetine. ***A-F.*** Representative poses of vortioxetine binding mode in the orthosteric binding site as observed in the docking clusters C2 (*A*), C6 (*B*), C8 (*C*), C11 (*D*), C13 (*E*), and C30 (*F*). Predicted interactions between the charged amine on the piperazine ring of vortioxetine and the protein are indicated with dashed lines. The key principal and complimentary subunit residues are colored in *white* and *gray*, respectively. Residue numbering refers to the h5-HT_{3A} sequence.

Molecular Pharmacology Fast Forward. Published on September 26, 2018 as DOI: 10.1124/mol.118.113530
This article has not been copyedited and formatted. The final version may differ from this version.

Figure 4. Ligand stability in the orthosteric binding site during MD simulations. ***A-F.*** Overlay of vortioxetine structure before (*cyan*) and after (*blue*) 52 ns of MD simulation of vortioxetine in cluster C2 (*A*), C6 (*B*), C8 (*C*), C11 (*D*), C13 (*E*), and C30 (*F*). The structural presentation is equivalent to Fig. 3. Time course of vortioxetine movement (calculated as the RMSD of vortioxetine orientation relative to initial conformation) are shown below panels. Smoothed data is shown in *dark blue*, while raw data is shown in *light blue*.

Figure 5. Electrophysiological characterization of vortioxetine activity. ***A***. Current traces from a representative *Xenopus* oocyte expressing h5-HT_{3A} in response to brief 20 s applications of 10 μM 5-HT (*black bar*) and 10 μM vortioxetine (*gray bar*). Vortioxetine causes rapidly desensitizing inward currents followed by a persistent inhibition. ***B-C***. Representative h5-HT_{3A} receptor current responses to extended application of 1 mM 5-HT (*black bar*; 500 s) and 10 μM vortioxetine (*gray bar*; 50 s). The mean ± SEM for the rate of desensitization (τ_{des}) was for vortioxetine $\tau_{des} = 7 \pm 4$ s (SEM; $n = 4$) and for 5-HT $\tau_{des} = 124 \pm 25$ s (SEM; $n = 4$).

Figure 6. Pharmacological characterization of vortioxetine in *Xenopus* oocytes and HEK-293 cells. ***A.*** Representative trace of fluorescence responses in HEK-293 cells expressing h5-HT_{3A} cells to the indicated concentration of 5-HT in μM using the membrane potential assay (*Materials and Methods*). ***B***. Representative current responses to the indicated concentration of 5-HT (μM) in *Xenopus* oocytes expressing h5-$HT3_A$ receptors at -20 mV. ***C-D.*** Concentration-response curves for 5-HT at *Xenopus* oocytes (*C*) and HEK-293 cells (*D*) expressing h5-HT_{3A}. Data points represent the normalized mean ± SD response from 5 to 10 individual experiments or oocytes for

Molecular Pharmacology Fast Forward. Published on September 26, 2018 as DOI: 10.1124/mol.118.113530
This article has not been copyedited and formatted. The final version may differ from this version.

each concentration. ***E***. Representative trace of fluorescence responses in HEK-293 cells expressing h5-HT_{3A} receptors to 30 μM 5-HT following incubation with the indicated concentration of vortioxetine using the membrane potential assay (*Materials and Methods*). ***F***. Concentration-response curves for vortioxetine inhibition of h5-HT_{3A} receptors at different concentrations of 5-HT. Data points represent the mean ± SD from 3 individual experiments. ***G.*** Concentration-inhibition curve for vortioxetine displacement of [^{3}H]GR65630 binding at membranes isolated from HEK-293 cells expressing h5-HT_{3A} (*Materials and Methods*). Data points represent mean ± SD from at least 3 individual experiments. ***E***. Saturation analysis of [^{3}H]vortioxetine binding at cell membranes isolated from HEK-293 cells expressing h5-HT_{3A}.

Figure 7. Mutational analysis of vortioxetine binding**.** ***A*.** Overview of key residues in the orthosteric binding site and vortioxetine orientation in the C11 (*blue*) and C13 (*cyan*) binding modes following short MD simulations. Mutated residues are labelled in *red.* Stick representations of residues where mutation resulted in decreased vortioxetine potency (Thr176 and Val202) are shown in *pale red*, and residues, where mutation did not alter potency (Ile66, Asn123, and Met223), are shown in *pale yellow*. ***B-F***. Representative concentration-inhibition curves for point mutants at the indicated positions. Data points represent mean ± SD from at least 6 individual concentration-response experiments for each mutant.

Figure 8. Key features of the orthosteric binding site in h5-HT_{3A}. ***A***. Tube representation of the residues forming the aromatic box within the orthosteric binding site. All residues from the principal subunit are colored in *white*, while all residues from the complementary subunit are

Molecular Pharmacology Fast Forward. Published on September 26, 2018 as DOI: 10.1124/mol.118.113530
This article has not been copyedited and formatted. The final version may differ from this version.

colored in *gray*. ***B***. Surface illustration of the subpockets involved in agonist (*green*), antagonist (*red*), and vortioxetine (*yellow*). The surrounding protein structure is shown as transparent ribbons.

Molecular Pharmacology Fast Forward. Published on September 26, 2018 as DOI: 10.1124/mol.118.113530
This article has not been copyedited and formatted. The final version may differ from this version.

12. Tables

Table 1. Results from the IFD calculations of vortioxetine into the orthosteric binding site of h5-HT_{3A}.

Cluster	n[a]	avg Emodel[b]	avg Gscore[b]	avg IFDscore[b]
C2	24	-62.6 ± 7.1	-10.3 ± 0.9	-3139.0 ± 1.4
C6	23	-66.9 ± 10.1	-11.5 ± 1.1	3141.3 ± 1.6
C8	62	-68.4 ± 6.6	-10.3 ± 1.0	-3139.0 ± 1.4
C11	40	-64.1 ± 6.7	-10.4 ± 1.3	-3139.4 ± 1.8
C13	8	-64.1 ± 6.7	-10.4 ± 1.3	-3139.4 ± 1.8
C30	39	-70.3 ± 8.7	-10.7 ± 1.8	-3140.0 ± 2.0
Outliers	67	-	-	-

[a] Number of poses within cluster.

[b] Average Emodel, XP Gscore, and IFD scores are reported in kcal/mol. Data represent mean ± SD.

Molecular Pharmacology Fast Forward. Published on September 26, 2018 as DOI: 10.1124/mol.118.113530
This article has not been copyedited and formatted. The final version may differ from this version.

Table 2. MM-PBSA estimated binding free energies of vortioxetine for each binding cluster.

Cluster	ΔG_{bind} [a]	SD	$\Delta\Delta G_{bind}$ [b]	SD
C2	-168.8	0.8	-0.4	1.1
C6	-168.4	0.8	0	-
C8	-177.8	1.1	-9.4	1.4
C11	-179.3	0.6	-10.9	1.0
C13	-184.5	0.8	-16.2	1.1
C30	-173.7	1.1	-5,4	1.3

[a] Binding free energies were calculated based on 100 frames evenly extracted from the first 2 ns of simulation as described in *Materials and Methods,* and are reported in kcal/mol with standard deviations (SD).

[b] Relative binding free energies are reported relative to C6, which has the highest calculated binding free energy, in kcal/mol with SD.

Molecular Pharmacology Fast Forward. Published on September 26, 2018 as DOI: 10.1124/mol.118.113530
This article has not been copyedited and formatted. The final version may differ from this version.

Table 3. Rationale for mutagenesis of binding site residues and predicted impact of mutations on vortioxetine IC_{50} for binding mode clusters.

Residue	Potential binding role of side chain[a]	Cluster	Mutation	Predicted effect[a]	
				Ligand interaction	*IC_{50}*
D64	γ-COOH salt bridge with piperazine NH_2	C30	V	disruption	↑↑↑
I66	Interactions with phenyl A	C11, C13	A	disruption	↑
			L	minor effect	minor effect
N123	γ-NH_2 interaction with piperazine NH_2	C8	A	HB disruption	↑↑
			I	HB disruption	↑↑
			L	HB disruption	↑↑
	Side chain close to phenyl B	C2, C13	A	HF interaction	↓
			I	HF interaction	↓
			L	HF interaction	↓
T176	γ-OH HB interaction with piperazine NH_2	C8	A	HB disruption	↑
			V	HB disruption	↑
	Transient γ-OH HB interaction with piperazine NH_2	C11, C13	A	HB disruption	minor effect
			V	HB disruption	minor effect
S177	Side chain close to piperazine NH_2	C2	E	HB formation	↓↓
V202	Side chain distant from ligand	C2, C6, C8	A	no effect	no effect
			I	no effect	no effect
			L	no effect	no effect
	Side chain close to phenyl A	C11, C13	A	HF perturbation	↑
			I	HF perturbation	minor effect
			L	HF perturbation	minor effect
M223	Side chain close to Phenyl A	C30	I	HF interaction	↓
E231	δ-COOH salt bridge with piperazine NH_2	C6	I	disruption	↑↑↑

[a] HB, SB, and HF abbreviates a hydrogen bond, salt bridge, and hydrophobic interactions, respectively.

Molecular Pharmacology Fast Forward. Published on September 26, 2018 as DOI: 10.1124/mol.118.113530
This article has not been copyedited and formatted. The final version may differ from this version.

Table 4. 5-HT EC_{50} and vortioxetine IC_{50} values for WT and mutant h5-HT_{3A} receptors.

Mutant	5-HT EC_{50} [a] (μM)	n [b]	Fold Change	Vortioxetine IC_{50} [a] (nM)	n [b]	Fold Change
WT	0.19 [0.17; 0.21]	33	-	29 [25;34]	9	-
D64V	NF	3	-	-	-	-
I66A	0.32 [0.24;0.44]	3	1.7 [1.3;2.3]	52 [41;66]*	5	1.8 [1.4;2.3]
I66L	0.27 [0.25;0.29]	3	1.4 [1.3;1.5]	42 [35;50]*	5	1.4 [1.2;1.7]
N123A	1.8 [1.5;2.1]*	9	9.5 [8.2;11]	47 [40;56]*	7	1.6 [1.4;1.9]
N123I	NF	3	-	-	-	-
N123L	2.2 [1.4;3.4]*	4	12 [7.6;18]	23 [9;57]	3	0.8 [0.3;2.0]
T176A	2.2 [2.0;2.5]*	6	12 [11;13]	32 [28;37]	5	1.1 [1.0;1.3]
T176V	4.46 [3.83;5.19]*	7	23 [20;27]	146 [123;174]*	5	5.0 [4.2;6.0]
S177E	NF	3	-	-	-	-
V202A	6.16 [5.53;6.86]*	6	6.2 [5.5;6.9]	310 [252;386]*	8	10.7 [8.7;13.3]
V202I	0.27 [0.24;0.31]	4	0.27 [0.24;0.31]	37 [30;45]	7	1.3 [1.0;1.6]
V202L	0.05 [0.03;0.07]*	3	0.05 [0.03;0.07]	5 [4;6]*	11	0.2 [0.1;0.2]
M223I	0.12 [0.10;0.13]	3	0.12 [0.10;0.13]	20 [16;25]	5	0.7 [0.6;0.9]
E231I	NF	3	-	-	-	-

[a] EC_{50} and IC_{50} values were determined as described in *Methods and materials.* Numbers in brackets denote the 95% confidence intervals. [b]*n* denotes number of independent experiments. *P <0.01 versus WT.

Molecular Pharmacology Fast Forward. Published on September 26, 2018 as DOI: 10.1124/mol.118.113530
This article has not been copyedited and formatted. The final version may differ from this version.

13. Figures

Figure 1

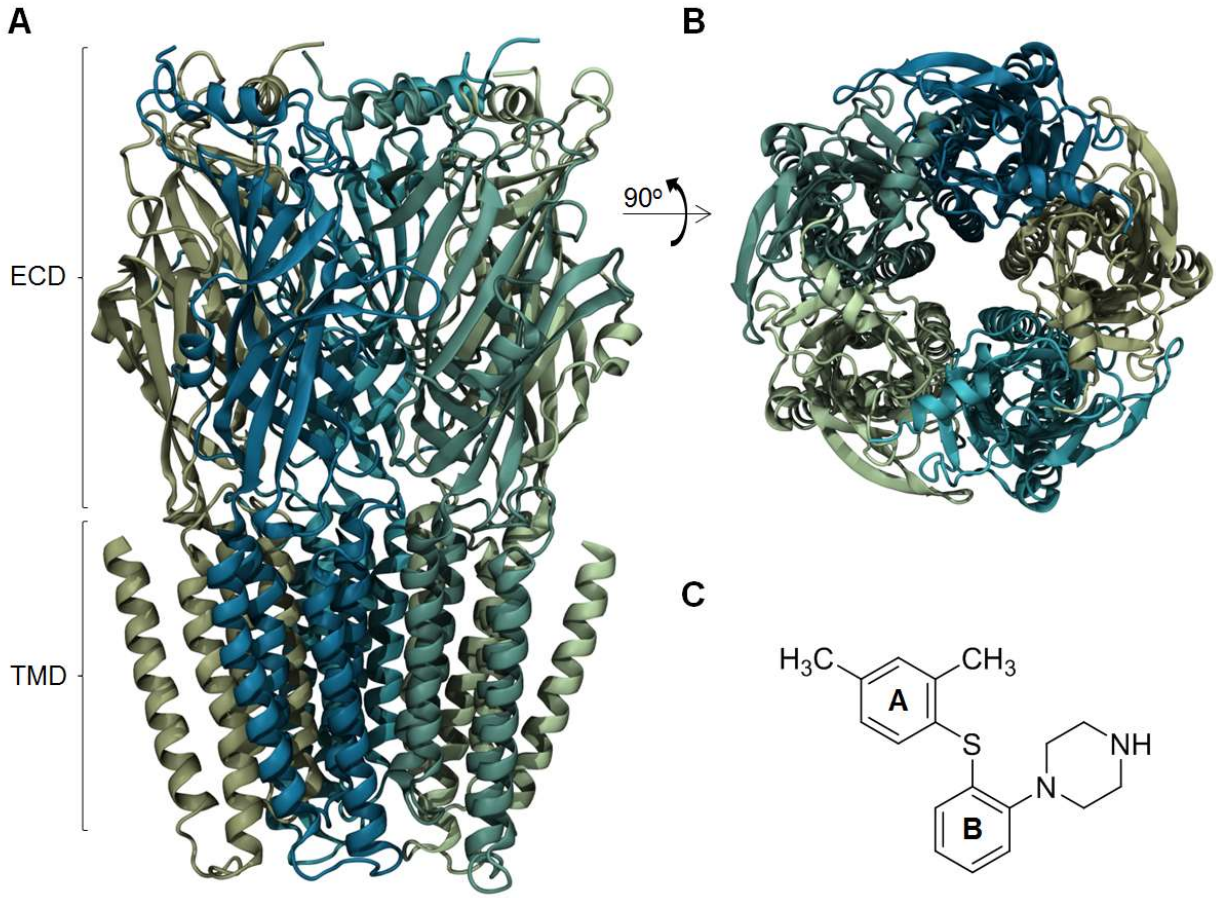

Molecular Pharmacology Fast Forward. Published on September 26, 2018 as DOI: 10.1124/mol.118.113530
This article has not been copyedited and formatted. The final version may differ from this version.

Figure 2

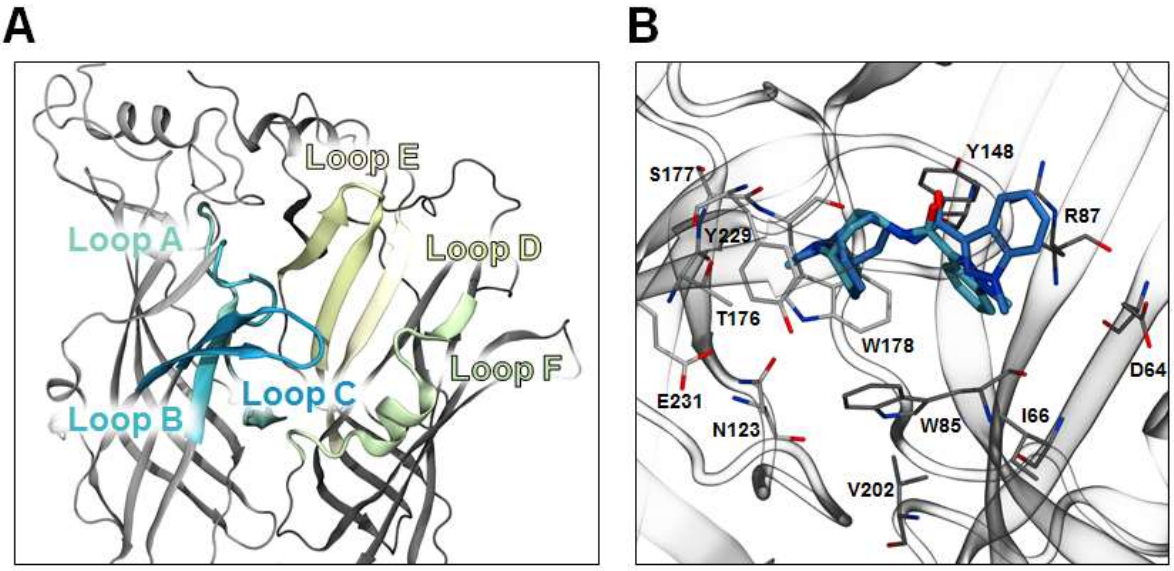

Molecular Pharmacology Fast Forward. Published on September 26, 2018 as DOI: 10.1124/mol.118.113530
This article has not been copyedited and formatted. The final version may differ from this version.

Figure 3

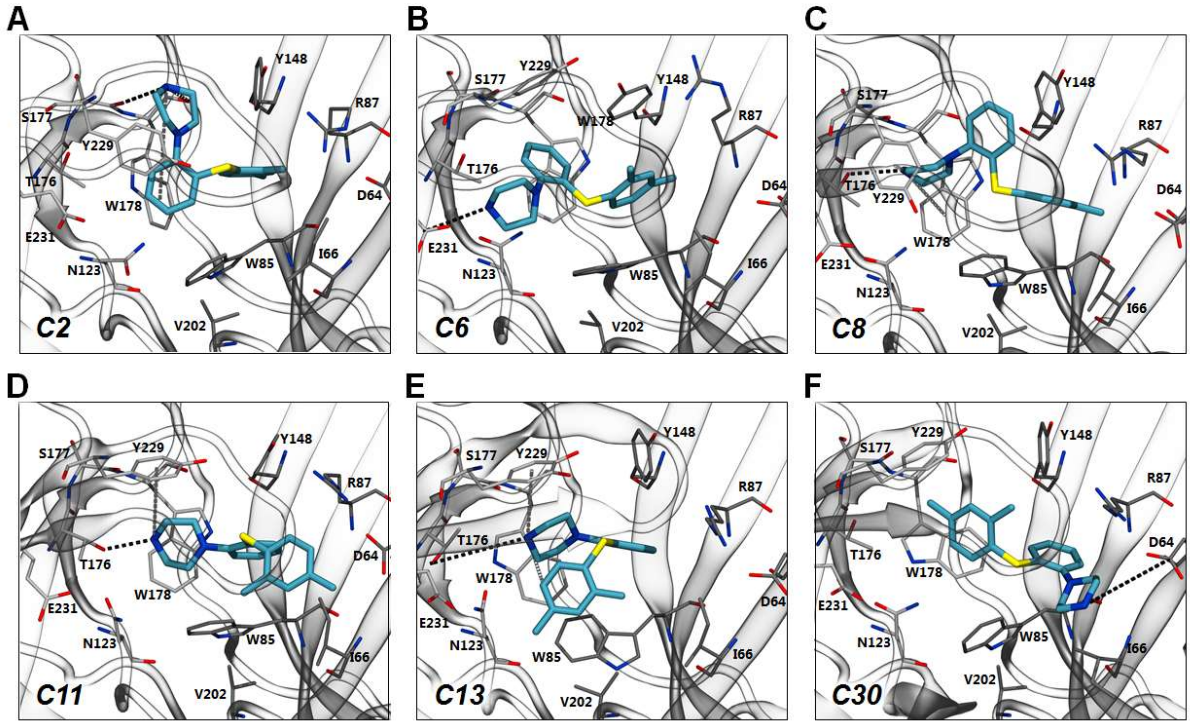

Molecular Pharmacology Fast Forward. Published on September 26, 2018 as DOI: 10.1124/mol.118.113530
This article has not been copyedited and formatted. The final version may differ from this version.

Figure 4

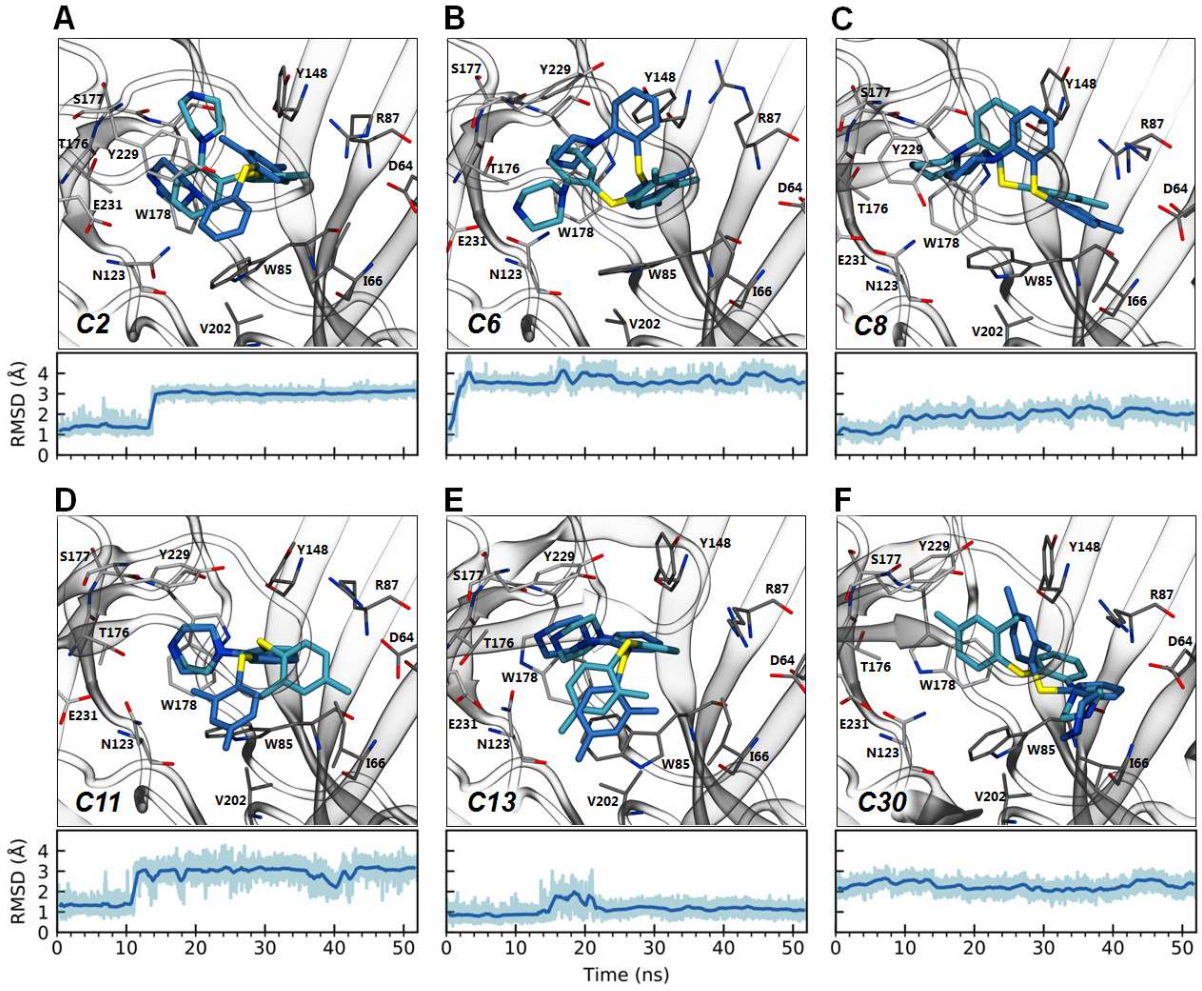

Molecular Pharmacology Fast Forward. Published on September 26, 2018 as DOI: 10.1124/mol.118.113530
This article has not been copyedited and formatted. The final version may differ from this version.

Figure 5

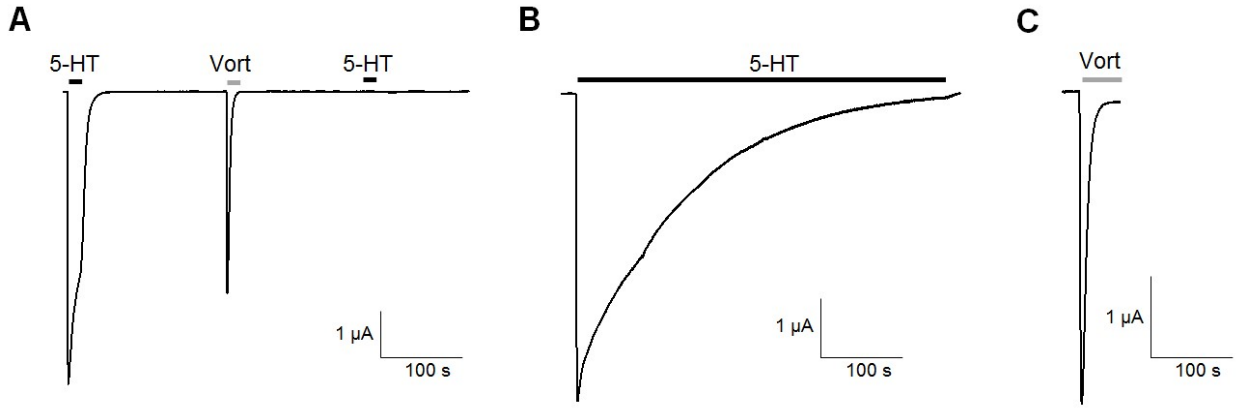

Molecular Pharmacology Fast Forward. Published on September 26, 2018 as DOI: 10.1124/mol.118.113530
This article has not been copyedited and formatted. The final version may differ from this version.

Figure 6

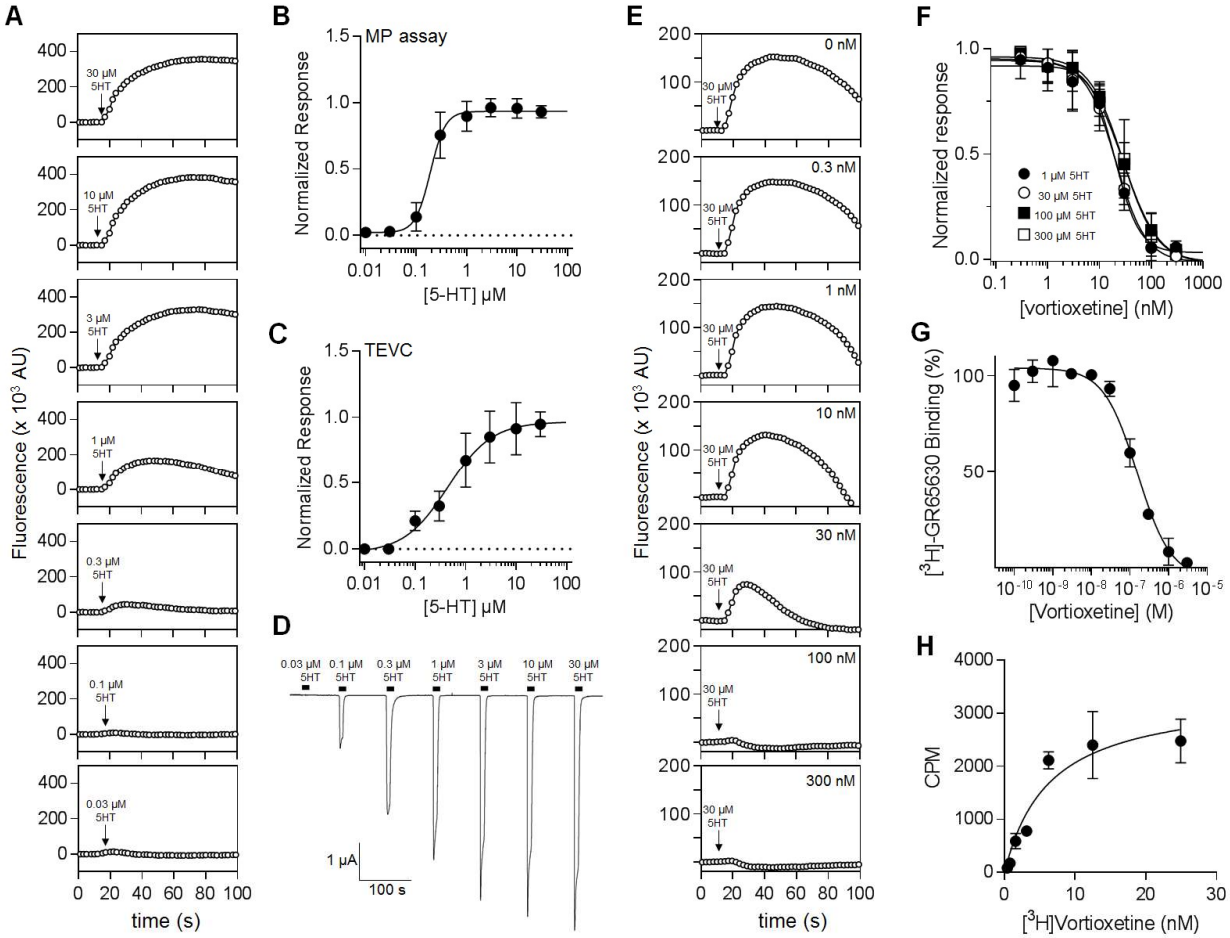

Molecular Pharmacology Fast Forward. Published on September 26, 2018 as DOI: 10.1124/mol.118.113530
This article has not been copyedited and formatted. The final version may differ from this version.

Figure 7

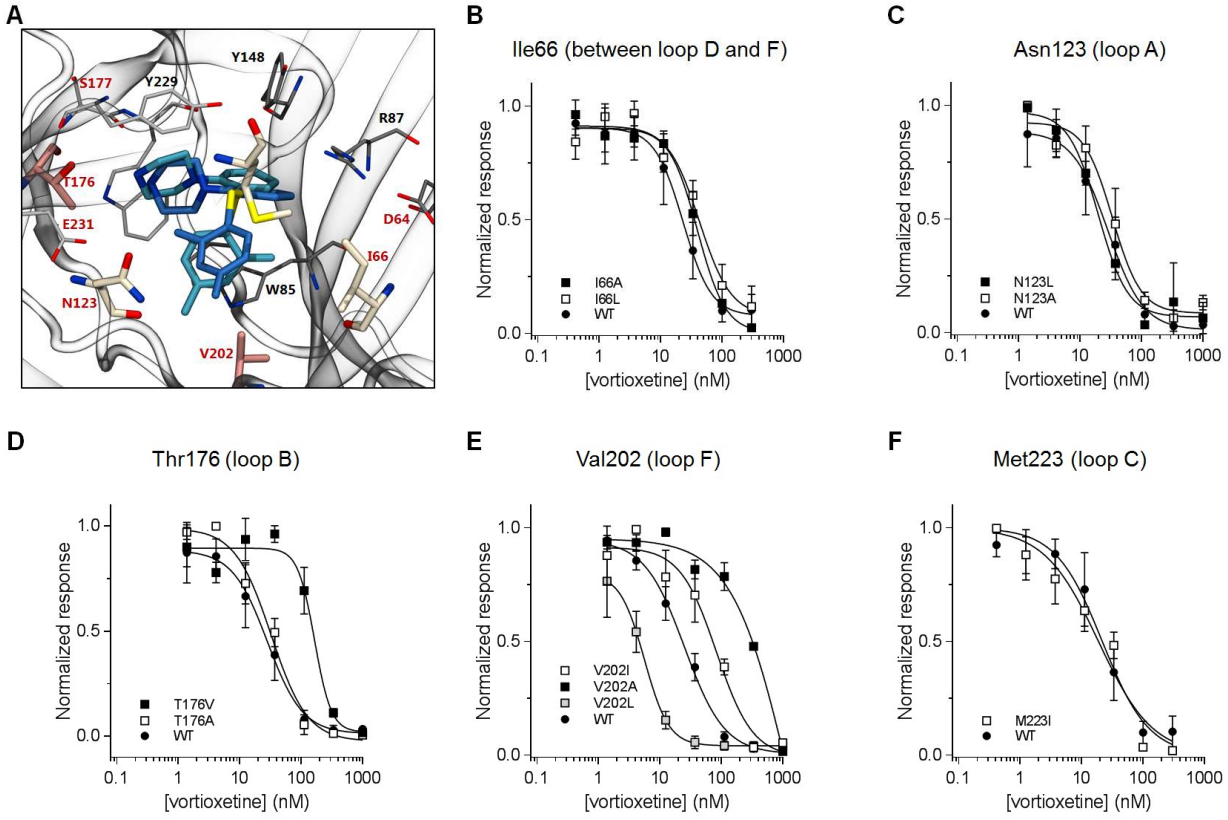

Molecular Pharmacology Fast Forward. Published on September 26, 2018 as DOI: 10.1124/mol.118.113530
This article has not been copyedited and formatted. The final version may differ from this version.

Figure 8

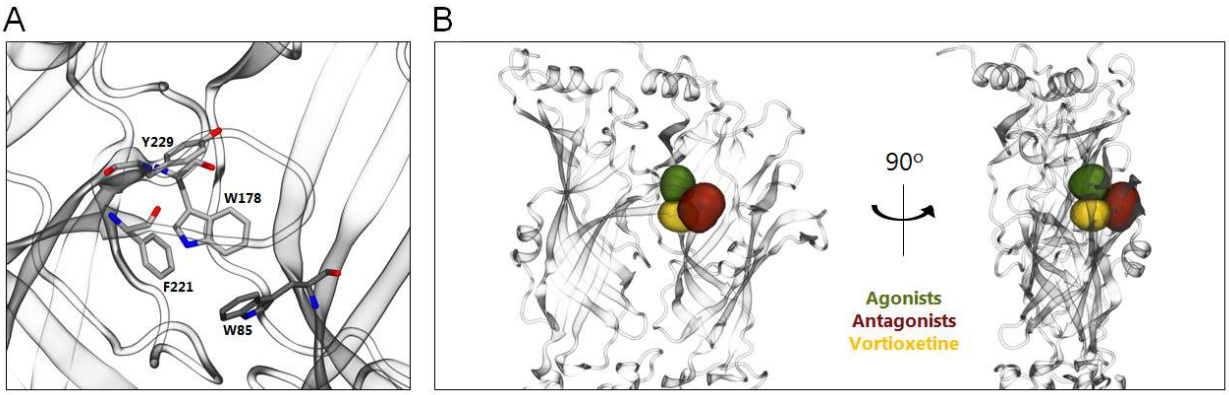

Supporting Information for

Modeling and mutational analysis of the binding mode for the multimodal antidepressant drug vortioxetine to the human 5-HT_{3A} receptor

Lucy Kate Ladefoged[1], Lachlan Munro[2], Anders Juel Pedersen[2], Benny Bang-Andersen[3], Thomas Balle[4], Birgit Schiøtt[1], Anders S. Kristensen[2]

[1]Interdisciplinary Nanoscience Center (iNANO), Department of Chemistry, Aarhus University, Langelandsgade 140, DK-8000 Aarhus, Denmark, [2]Department of Drug Design and Pharmacology, University of Copenhagen, Universitetsparken 2, DK-2100 Copenhagen, Denmark, [3]Lundbeck Research, Lundbeck A/S, Ottiliavej 9, DK-2500 Valby, Denmark, [4]Sydney School of Pharmacy, Faculty of Medicine and Health, The University of Sydney, Sydney, NSW 2006, Australia.

Figure S1. **Amino acid sequence alignment of h5-HT$_{3A}$, m5-HT$_{3A}$, hGABA$_A$ and aAChBP used for homology modeling of the h5-HT3A receptor**. The sequence segments applied as templates in the homology modeling of h5-HT$_{3A}$ are highlighted in *gray* for each of the three templates. PDB IDs for the structures corresponding to the sequences are shown in parenthesis. For h5-HT$_{3A}$, the code in parenthesis refers to the protein UniProt ID. The location of loop A-F and the transmembrane regions M1 to M4 are depicted on top of the alignment. Loops A to C are indicated in *green*, loops D to F are indicated in *turquoise*, the Cys-loop is indicated in *purple*, and the transmembrane segments are indicated in *blue*.

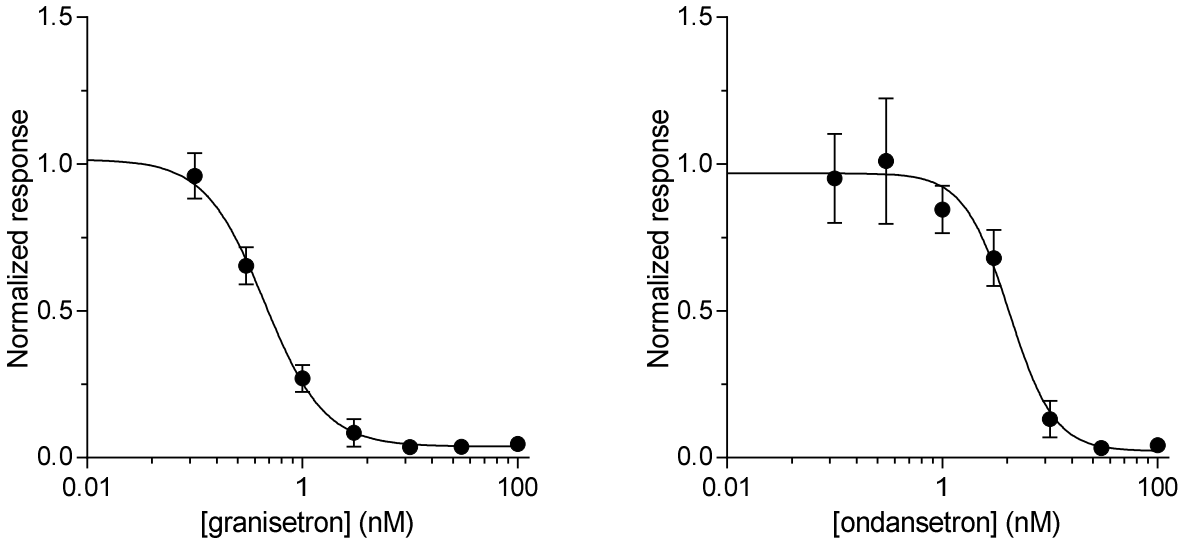

Figure S2. Determination of IC_{50} for the classical 5-HT_{3A} receptor competitive antagonist granisetron and ondansetron using the membrane potential assay. ***A-B***. Composite concentration-inhibition curves for granisetron (A) and ondansetron (*B*) constructed using the membrane potential assay (*Materials and Methods*). Data represent the mean + SEM from 5-8 independent experiments.

SUPPLEMENTARY METHODS

Protein modeling – We modeled the h5-HT_{3A} receptor in an inactive conformation here defined as the receptor having a closed channel with proposed gating residues obstructing ion passage, and the C loop moved away from the substrate binding site. We used as templates the mouse 5-HT_{3A} receptor (PDB ID: 4PIR, 86% sequence identity (seqID)) (Hassaine et al., 2014), the GABA receptor (PDB ID: 4COF, 23% seqID) (Miller and Aricescu, 2014), and 5-HTBP (PDB ID: 2YME, 22% seqID) (Kesters et al., 2013). Alignment of these template structures to the h5-HT_{3A} sequence was aided by a preexisting in-house alignment that contained sequences of all human pLGICs and all pLGICs receptors with available structures at the time of modeling (PDB IDs: 4COF, 3RIF, 3EAM, 2VL0, 2QC1, 2BYQ, 1UW6, and 2BJ0) (Bocquet et al., 2009; Celie et al., 2005; Celie et al., 2004; Dellisanti et al., 2007; Hansen et al., 2005; Hibbs and Gouaux, 2011; Hilf and Dutzler, 2008; Miller and Aricescu, 2014). The sequence of the h5-HT_{3A} subunit (UniProt ID: P46098) as well as the 5-HTBP sequence were added to the preexisting alignment using ClustalX version 2.0 (Larkin et al., 2007) and manually adjusted. Supporting figure S1 illustrates the sequence segments used from each template. Homology modeling was performed using MODELLER version 9.14 (Sali and Blundell, 1993). A total of 100 models were created, and the cysteine bridge in the cys-loop was patched during modeling. Granisetron was built into the model as found in the 5-HTBP template. The best models were chosen on the basis of molpdf and DOPE score (scoring functions in MODELLER), DOPE per residue plots, Ramachandran plot violations, protein-ligand interactions, binding site volume, and channel radius as assessed by the software Hole (Smart et al., 1996). The best model was selected for loop optimization and overall refinement. The M2M3 loop and residues E272 and L282 were optimized, and the M3M4 linker (residues QPAR) was altered to be equal to the longer linker region used in other crystal structures as to not bias the M4 conformation (residues AGTLRVGS) and was then optimized accordingly (residues 332-339). All geometry optimizations were performed using Prime version 3.7 (Jacobson et al., 2004). Loops were optimized using the extended sampling protocol and the OPLS-2005 force field (Kaminski et al., 2001), and side chains were optimized using the OPLS-2005 force field while backbone sampling of the direct neighboring residues was allowed. The final models consisted of

residues 30-475 with the exception of the ICD (residues 332-447) and contained a bound granisetron molecule in each site. In order to relax the h5-HT_{3A} model before docking calculations it was submitted to molecular dynamics (MD) simulations for 10 ns with Cα atoms positionally restrained. In preparation for MD simulation, the protonation states of relevant residues were assessed using PROPKA version 3.0 (Olsson et al., 2011) and manual evaluation. A cysteine bridge was modelled in the name-giving cys-loop between C157 and C171 (Lummis, 2012). All aspartic and glutamic acids were modelled in deprotonated states and all histidine residues were modelled as the delta tautomer.

Molecular dynamics simulations – Simulation systems were prepared using the modeled *apo* structure of h5-HT_{3A} prepared for docking calculations or the vortioxetine bound structure from the C2 docking cluster. Proteins containing a representative vortioxetine structure from the remaining clusters were directly placed into an atomistic membrane patch prepared for the C2 cluster, thus skipping the coarse grained (CG) steps and equilibrating all systems in all atom (AA) using different initial velocities as described below. The *apo*/representative C2 structure was converted into its CG equivalent and placed in a crystalline-like CG 1-palmitoyl-2-oleoyl-sn-glycero-3-phosphocholine (POPC) bilayer with water and 0.2 M NaCl above and below it using the Martinize and Insane tools (Wassenaar et al., 2015). The system was then minimized using the Martini 2.2 force field (de Jong et al., 2013) using a steepest descent algorithm for 500,000 steps or until convergence, followed by a 0.5 ns MD simulation in the NVT ensemble using the velocity rescale algorithm to control the temperature at 310 K and a 10 fs time step with the protein restrained. Electrostatics were calculated using the reaction field method with a cut-off of 11 Å with a dielectric constant of 0 (=infinite) when beyond the cut-off, while vdW interactions were treated with a cut-off of 11 Å in combination with the potential-shift-verlet modifier. A 5 ns MD simulation in the NPT ensemble was then performed using the same settings, but with the addition of coupling to a Berendsen semi-isotropic pressure bath to control the pressure at 1 bar. The whole system was then converted into its all atom (AA) equivalent and to ensure the correct starting conformation of the protein, the backmapped protein structure (using the Backward tool (Wassenaar et al., 2014))

was swapped for the original, prepared structure. The now AA system was then minimized with protein restraints (k=1000 kJ mol^{-1} nm^{-2}) using the CHARMM36 force field for the protein and lipids (Best et al., 2012; Klauda et al., 2010; MacKerell et al., 1998) and the TIPS3P water model (Durell et al., 1994) followed by a full minimization without restraints using a steepest descent algorithm for 500,000 steps or until convergence. The parameters used for vortioxetine are described below. The system was then equilibrated; first in the NVT ensemble for 0.5 ns using a 1 fs time step, and then in the NPT ensemble for 1 ns using a 2 fs time step. Both ensembles were sampled with restraints on ligand and C_α atoms (k=1000 kJ mol^{-1} nm^{-2}) While in the NVT ensemble the velocity rescale thermostat was applied to control the temperature at 310 K, while in the NPT ensemble the Nosé-Hoover thermostat was applied in combination with the Parrinello-Rahman barostat (semi-isotropic scaling) to control the temperature and pressure at 310 K and 1 bar, respectively. In both ensembles electrostatics were treated with the Verlet cut-off scheme using a 12 Å radius while the long-range electrostatic interactions were calculated using the Particle Mesh Ewald algorithm. The vdW interactions were calculated using cut-offs at 12 Å with a force modifier applied from 10 Å. All bonds to hydrogen atoms were restrained using the LINCS algorithm (Hess et al., 1997). The system involving the *apo* protein was simulated for 10 ns with restraints on C_α atoms after equilibration as a preparation for the docking calculations, while the systems containing vortioxetine bound proteins were each simulated for 2+50 ns with restraints on C_α atoms (ligand unrestrained pre-production equilibration and production run, respectively). Restraints were applied during pre-production and production runs, as the pore region was observed to desolvate due to small changes in protein structure. The simulation data collected during the pre-production equilibration run was included in the data analysis as it was observed that the binding mode of vortioxetine changed dramatically during the first 2 ns of simulations in some clusters. The simulated systems contained ~270.000 atoms and had a box size of ~119x114x195 $Å^3$. All simulations were performed in Gromacs version 5.0.2 (Pronk et al., 2013).

Vortioxetine parameters. Parameters for vortioxetine were initially found using the paramchem webserver (https://cgenff.paramchem.org/) which selects parameters based on analogy

to existing parameters in the CHARMM36 and CGenFF force fields (Best et al., 2012; Klauda et al., 2010; MacKerell et al., 1998; Vanommeslaeghe et al., 2010; Vanommeslaeghe and MacKerell, 2012; Vanommeslaeghe et al., 2012; Yu et al., 2012). Based on the associated penalty scores a subset of parameters were deemed unsatisfactory and were parameterized from scratch using the force field tool-kit (ffTK) (Mayne et al., 2013) The unsatisfactory parameters consist of stretch and bend parameters for atoms bound to the neutral nitrogen in the piperazine ring as well as the dihedral parameters involving the piperazine ring and the sulfur atom. ffTK assisted in producing Gaussian 09 (M. J. Frisch, 2016) input files in a manner consistent with the CHARMM parameterization protocol as well as in the fitting and evaluation of the produced parameters. The fitted parameters were further evaluated using MD simulations of vortioxetine in water in which the conformations visited by vortioxetine were assessed and compared to the conformations found to be most common in QM calculations at the MP2 level of theory. The conformations were also compared to a conformational search of vortioxetine using the OPLS2.1 force field, and both force fields find the same conformations (data not shown). The resulting parameters are available upon request.

SUPPLEMENTARY REFERENCES

Best RB, Zhu X, Shim J, Lopes PEM, Mittal J, Feig M and MacKerell AD (2012) Optimization of the Additive CHARMM All-Atom Protein Force Field Targeting Improved Sampling of the Backbone phi, psi and Side-Chain chi(1) and chi(2) Dihedral Angles. *J Chem Theory Comput* **8**(9): 3257-3273.

Bocquet N, Nury H, Baaden M, Le Poupon C, Changeux JP, Delarue M and Corringer PJ (2009) X-ray structure of a pentameric ligand-gated ion channel in an apparently open conformation. *Nature* **457**(7225): 111-114.

Celie PHN, Klaassen RV, van Rossum-Fikkert SE, van Elk R, van Nierop P, Smit AB and Sixma TK (2005) Crystal structure of acetylcholine-binding protein from Bulinus truncatus reveals the conserved structural scaffold and sites of variation in nicotinic acetylcholine receptors. *J Biol Chem* **280**(28): 26457-26466.

Celie PHN, van Rossum-Fikkert SE, van Dijk WJ, Brejc K, Smit AB and Sixma TK (2004) Nicotine and carbamylcholine binding to nicotinic acetylcholine receptors as studied in AChBP crystal structures. *Neuron* **41**(6): 907-914.

de Jong DH, Singh G, Bennett WFD, Arnarez C, Wassenaar TA, Schafer LV, Periole X, Tieleman DP and Marrink SJ (2013) Improved Parameters for the Martini Coarse-Grained Protein Force Field. *J Chem Theory Comput* **9**(1): 687-697.

Dellisanti CD, Yao Y, Stroud JC, Wang ZZ and Chen L (2007) Crystal structure of the extracellular domain of nAChR alpha 1 bound to alpha-bungarotoxin at 1.94 angstrom resolution (vol 10, pg 953, 2007). *Nat Neurosci* **10**(9): 1222-1222.

Durell SR, Brooks BR and Bennaim A (1994) Solvent-Induced Forces between 2 Hydrophilic Groups. *J Phys Chem-Us* **98**(8): 2198-2202.

Hansen SB, Sulzenbacher G, Huxford T, Marchot P, Taylor P and Bourne Y (2005) Structures of Aplysia AChBP complexes with nicotinic agonists and antagonists reveal distinctive binding interfaces and conformations. *Embo Journal* **24**(20): 3635-3646.

Hassaine G, Deluz C, Grasso L, Wyss R, Tol MB, Hovius R, Graff A, Stahlberg H, Tomizaki T, Desmyter A, Moreau C, Li XD, Poitevin F, Vogel H and Nury H (2014) X-ray structure of the mouse serotonin 5-HT3 receptor. *Nature* **512**(7514): 276-+.

Hess B, Bekker H, Berendsen HJC and Fraaije JGEM (1997) LINCS: A linear constraint solver for molecular simulations. *J Comput Chem* **18**(12): 1463-1472.

Hibbs RE and Gouaux E (2011) Principles of activation and permeation in an anion-selective Cys-loop receptor. *Nature* **474**(7349): 54-U80.

Hilf RJ and Dutzler R (2008) X-ray structure of a prokaryotic pentameric ligand-gated ion channel. *Nature* **452**(7185): 375-379.

Jacobson MP, Pincus DL, Rapp CS, Day TJF, Honig B, Shaw DE and Friesner RA (2004) A hierarchical approach to all-atom protein loop prediction. *Proteins* **55**(2): 351-367.

Kaminski GA, Friesner RA, Tirado-Rives J and Jorgensen WL (2001) Evaluation and reparametrization of the OPLS-AA force field for proteins via comparison with accurate quantum chemical calculations on peptides. *J Phys Chem B* **105**(28): 6474-6487.

Kesters D, Thompson AJ, Brams M, van Elk R, Spurny R, Geitmann M, Villalgordo JM, Guskov A, Danielson UH, Lummis SCR, Smit AB and Ulens C (2013) Structural basis of ligand recognition in 5-HT3 receptors. *Embo Rep* **14**(1): 49-56.

Klauda JB, Venable RM, Freites JA, O'Connor JW, Tobias DJ, Mondragon-Ramirez C, Vorobyov I, MacKerell AD and Pastor RW (2010) Update of the CHARMM All-Atom Additive Force Field for Lipids: Validation on Six Lipid Types. *J Phys Chem B* **114**(23): 7830-7843.

Larkin MA, Blackshields G, Brown NP, Chenna R, McGettigan PA, McWilliam H, Valentin F, Wallace IM, Wilm A, Lopez R, Thompson JD, Gibson TJ and Higgins DG (2007) Clustal W and clustal X version 2.0. *Bioinformatics* **23**(21): 2947-2948.

Lummis SCR (2012) 5-HT3 Receptors. *J Biol Chem* **287**(48): 40239-40245.

M. J. Frisch GWT, H. B. Schlegel, G. E. Scuseria, M. A. Robb, J. R. Cheeseman, G. Scalmani, V. Barone, G. A. Petersson, H. Nakatsuji, X. Li, M. Caricato, A. Marenich, J. Bloino, B. G. Janesko, R. Gomperts, B. Mennucci, H. P. Hratchian, J. V. Ortiz, A. F. Izmaylov, J. L. Sonnenberg, D. Williams-Young, F. Ding, F. Lipparini, F. Egidi, J. Goings, B. Peng, A. Petrone, T. Henderson, D. Ranasinghe, V. G. Zakrzewski, J. Gao, N. Rega, G. Zheng, W. Liang, M. Hada, M. Ehara, K. Toyota, R. Fukuda, J. Hasegawa, M. Ishida, T. Nakajima, Y. Honda, O. Kitao, H. Nakai, T. Vreven, K. Throssell, J. A. Montgomery, Jr., J. E. Peralta, F. Ogliaro, M. Bearpark, J. J. Heyd, E. Brothers, K. N. Kudin, V. N. Staroverov, T. Keith, R. Kobayashi, J. Normand, K. Raghavachari, A. Rendell, J. C. Burant, S. S. Iyengar, J. Tomasi, M. Cossi, J. M. Millam, M. Klene, C. Adamo, R. Cammi, J. W.

Ochterski, R. L. Martin, K. Morokuma, O. Farkas, J. B. Foresman, and D. J. Fox, (2016) Gaussian 09, Gaussian Inc., Wallingford CT.

MacKerell AD, Bashford D, Bellott M, Dunbrack RL, Evanseck JD, Field MJ, Fischer S, Gao J, Guo H, Ha S, Joseph-McCarthy D, Kuchnir L, Kuczera K, Lau FTK, Mattos C, Michnick S, Ngo T, Nguyen DT, Prodhom B, Reiher WE, Roux B, Schlenkrich M, Smith JC, Stote R, Straub J, Watanabe M, Wiorkiewicz-Kuczera J, Yin D and Karplus M (1998) All-atom empirical potential for molecular modeling and dynamics studies of proteins. *J Phys Chem B* **102**(18): 3586-3616.

Mayne CG, Saam J, Schulten K, Tajkhorshid E and Gumbart JC (2013) Rapid Parameterization of Small Molecules Using the Force Field Toolkit. *J Comput Chem* **34**(32): 2757-2770.

Miller PS and Aricescu AR (2014) Crystal structure of a human GABA(A) receptor. *Nature* **512**(7514): 270-+.

Olsson MHM, Søndergaard CR, Rostkowski M and Jensen JH (2011) PROPKA3: Consistent Treatment of Internal and Surface Residues in Empirical pK(a) Predictions. *J Chem Theory Comput* **7**(2): 525-537.

Pronk S, Pall S, Schulz R, Larsson P, Bjelkmar P, Apostolov R, Shirts MR, Smith JC, Kasson PM, van der Spoel D, Hess B and Lindahl E (2013) GROMACS 4.5: a high-throughput and highly parallel open source molecular simulation toolkit. *Bioinformatics* **29**(7): 845-854.

Sali A and Blundell TL (1993) Comparative Protein Modeling by Satisfaction of Spatial Restraints. *Journal of molecular biology* **234**(3): 779-815.

Smart OS, Neduvelil JG, Wang X, Wallace BA and Sansom MS (1996) HOLE: a program for the analysis of the pore dimensions of ion channel structural models. *Journal of molecular graphics* **14**(6): 354-360, 376.

Vanommeslaeghe K, Hatcher E, Acharya C, Kundu S, Zhong S, Shim J, Darian E, Guvench O, Lopes P, Vorobyov I and MacKerell AD (2010) CHARMM General Force Field: A Force Field for Drug-Like Molecules Compatible with the CHARMM All-Atom Additive Biological Force Fields. *J Comput Chem* **31**(4): 671-690.

Vanommeslaeghe K and MacKerell AD (2012) Automation of the CHARMM General Force Field (CGenFF) I: Bond Perception and Atom Typing. *J Chem Inf Model* **52**(12): 3144-3154.

Vanommeslaeghe K, Raman EP and MacKerell AD (2012) Automation of the CHARMM General Force Field (CGenFF) II: Assignment of Bonded Parameters and Partial Atomic Charges. *J Chem Inf Model* **52**(12): 3155-3168.

Wassenaar TA, Ingolfsson HI, Bockmann RA, Tieleman DP and Marrink SJ (2015) Computational Lipidomics with insane: A Versatile Tool for Generating Custom Membranes for Molecular Simulations. *J Chem Theory Comput* **11**(5): 2144-2155.

Wassenaar TA, Pluhackova K, Bockmann RA, Marrink SJ and Tieleman DP (2014) Going Backward: A Flexible Geometric Approach to Reverse Transformation from Coarse Grained to Atomistic Models. *J Chem Theory Comput* **10**(2): 676-690.

Yu WB, He XB, Vanommeslaeghe K and MacKerell AD (2012) Extension of the CHARMM general force field to sulfonyl-containing compounds and its utility in biomolecular simulations. *J Comput Chem* **33**(31): 2451-2468.